Cell Reports

Article

The Rb/E2F axis is a key regulator of the molecular signatures instructing the quiescent and activated adult neural stem cell state

Graphical abstract

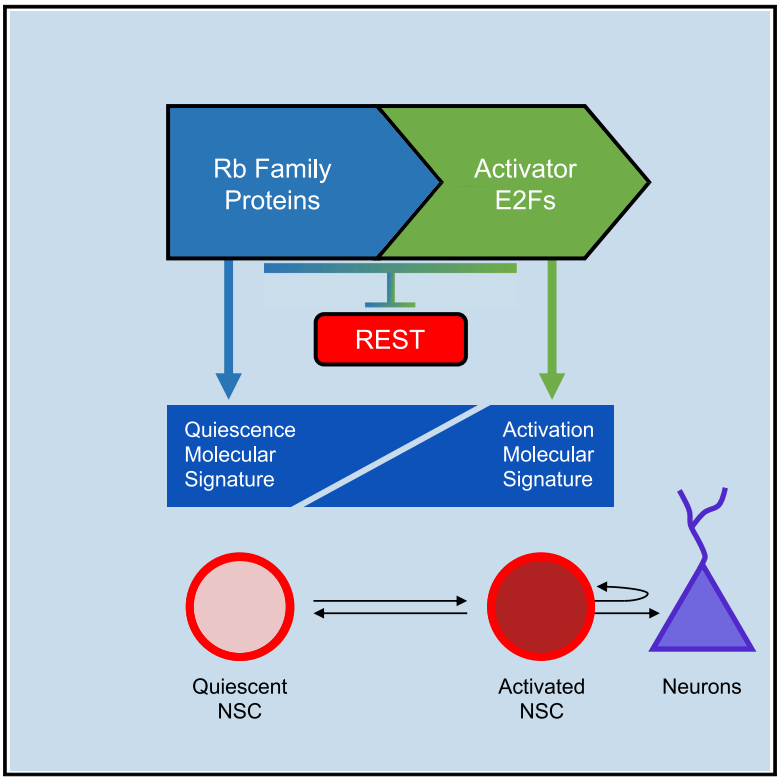

Highlights

- The Rb/E2F axis coordinates cell-cycle control with NSC activation and quiescence
- The Rb/E2F axis is required for neurogenesis and NSC maintenance in the subgranular zone
- The Rb/E2F axis is required for regulation of factors essential for NSC function

Authors

Bensun C. Fong, Imane Chakroun, Mohamed Ariff Iqbal, ..., Noël Ghanem, Renaud Vandenbosch, Ruth S. Slack

Correspondence

rvandenbosch@uliege.be (R.V.), rslack@uottawa.ca (R.S.S.)

In brief

Maintenance of adult neural stem cells (NSCs) and neurogenesis depends on proper regulation of activation and quiescence of NSCs. How these transitions are coordinated with the cell cycle is unclear. Fong et al. show that the Rb/E2F axis links the cell-cycle machinery to master regulators of NSC fate.

Fong et al., 2022, Cell Reports *41*, 111578
November 1, 2022
https://doi.org/10.1016/j.celrep.2022.111578

CellPress

Cell Reports

CellPress
OPEN ACCESS

Article

The Rb/E2F axis is a key regulator of the molecular signatures instructing the quiescent and activated adult neural stem cell state

Bensun C. Fong,[1] Imane Chakroun,[1] Mohamed Ariff Iqbal,[1] Smitha Paul,[1] Joseph Bastasic,[1] Daniel O'Neil,[1] Edward Yakubovich,[1] Anthony T. Bejjani,[6] Nastaran Ahmadi,[1] Anthony Carter,[1] Alysen Clark,[1] Gustavo Leone,[2] David S. Park,[3,4,5] Noël Ghanem,[6] Renaud Vandenbosch,[7,8,*] and Ruth S. Slack[1,9,*]

[1]University of Ottawa Brain and Mind Research Institute, Department of Cellular and Molecular Medicine, University of Ottawa, Ottawa, ON K1H 8M5, Canada
[2]MCW Cancer Centre, Medical College of Wisconsin, Milwaukee, WI, USA
[3]Department of Clinical Neurosciences, University of Calgary, Calgary, AB T2N 4N1, Canada
[4]Department of Cell Biology, University of Calgary, Calgary, AB T2N 4N1, Canada
[5]Department of Anatomy, University of Calgary Calgary AB T2N 4N1 Canada
[6]Department of Biology, American University of Beirut, PO Box 11-0236, Riad El Solh, Beirut 1107 2020, Lebanon
[7]Laboratory of Developmental Neurobiology, GIGA Stem Cells & GIGA Neurosciences, University of Liège, Liège, Belgium
[8]Division of Histology, Department of Biomedical and Preclinical Sciences, University of Liège, Liège, Belgium
[9]Lead contact
*Correspondence: rvandenbosch@uliege.be (R.V.), rslack@uottawa.ca (R.S.S.)
https://doi.org/10.1016/j.celrep.2022.111578

SUMMARY

Long-term maintenance of the adult neurogenic niche depends on proper regulation of entry and exit from quiescence. Neural stem cell (NSC) transition from quiescence to activation is a complex process requiring precise cell-cycle control coordinated with transcriptional and morphological changes. How NSC fate transitions in coordination with the cell-cycle machinery remains poorly understood. Here we show that the Rb/E2F axis functions by linking the cell-cycle machinery to pivotal regulators of NSC fate. Deletion of Rb family proteins results in activation of NSCs, inducing a transcriptomic transition toward activation. Deletion of their target activator E2Fs1/3 results in intractable quiescence and cessation of neurogenesis. We show that the Rb/E2F axis mediates these fate transitions through regulation of factors essential for NSC function, including REST and ASCL1. Thus, the Rb/E2F axis is an important regulator of NSC fate, coordinating cell-cycle control with NSC activation and quiescence fate transitions.

INTRODUCTION

Compelling evidence reveals that neurogenesis, which occurs in the adult mammalian brain, plays an important role in memory and cognition and has therapeutic potential for endogenous repair (Gonçalves et al., 2016). Generation of neurons throughout life depends on long-term maintenance of a population of quiescent neural stem cells (NSCs), which reside in defined niches. Critical for this process is the ability to maintain and effectively regulate NSC entry and exit from quiescence. The dynamic transition from quiescence to activation is a complex process requiring not only precise cell cycle control but also a coordinated phenotypic transition involving transcriptional and morphological changes (Urbán et al., 2019). Single-cell transcriptomics studies have shown that NSCs progressing between states of quiescence and activation possess distinct gene expression profiles essential for NSCs to maintain a quiescent state and competence to respond to niche environmental cues. Quiescent NSCs are enriched in cell signaling, communication, and adhesion genes, and activated NSCs express a repertoire of genes necessary for activation, including ribosomal and RNA synthesis as well as DNA replication and repair (Basak et al., 2018; Codega et al., 2014). It remains elusive how such a complex repertoire of factors interacts and functions in a coordinated manner with the core cell cycle machinery to mediate these critical NSC fate transitions.

The retinoblastoma gene Rb was the first tumor suppressor gene to be cloned (Friend et al., 1986; Lee et al., 1987) and has been intensively studied in the field of oncogenesis. Although Rb family proteins have been shown to interact with multiple cellular factors, the best known binding partners are the E2F family of transcription factors through which the Rb family regulates G1-S transition. Three Rb family proteins have overlapping functions (pRb, p107, and p130) and interact with E2Fs to regulate proliferation, self-renewal, and onset of differentiation. We and others have shown that the Rb family members and their regulatory targets control expression of pluripotency factors such as Sox2 (Julian et al., 2013; Kareta et al., 2015). Studies

have identified an essential role of the Rb family in regulating hematopoietic stem cell homeostasis by repressing tissue-specific E2F targets (Kim et al., 2017; Viatour et al., 2008).

Here we show that the Rb/E2F pathway is a key regulator of NSC fate by coordinating the transcriptional program that controls quiescence and activation. We show that the Rb/E2F axis functions as an on-off switch for NSC quiescence and activation by linking the cell cycle machinery to pivotal regulators of NSC fate. Compound deletion of Rb family proteins results in activation and expansion of NSCs and induces a transcriptomic transition toward NSC activation, followed by niche depletion in the subgranular zone (SGZ) of the dentate gyrus (DG). In contrast, deletion of the activator E2Fs E2F1 and E2F3 results in failure of NSCs to undergo activation and acquisition of a transcriptome associated with intractable NSC quiescence. The Rb/E2F axis mediates these fate transitions by regulating factors essential for NSC function, including REST and ASCL1. This makes the Rb/E2F axis an important regulator of NSC fate, coordinating cell cycle control with NSC activation and quiescence fate transitions.

RESULTS

Our previous results revealed that Rb is required to regulate proliferation and survival of committed neuroblasts in the adult brain (Naser et al., 2016; Vandenbosch et al., 2016); however, Rb itself is dispensable for regulating the function of the adult NSC population. Given that cell cycle regulation is a crucial requirement to control NSC quiescence and long-term maintenance, we wanted to determine whether there is redundancy in Rb family protein function and whether these pocket proteins play a critical role in regulation of the NSC population. To test this, we used tamoxifen (Tam)-inducible NestinCreER^{T2};R26-eYFP mice to conditionally delete Rb and p130 in adult NSCs together with a germline deletion of p107 (Rb-TKO). Mice triple-heterozygous for the Rb family (Rb-THC), which exhibited a phenotype similar to wild-type animals (Figure S1A), were used as littermate controls.

In the SGZ, Rb family loss results in a dramatic 6.3-fold expansion of the total YFP+ recombined cell population, 4 weeks post Tam (wpi) (Figure 1A). This population, 75% labeled with the proliferation marker Ki67, is comprised of over 80% Sox2-expressing cells, suggesting that Rb family proteins are essential to maintain NSC quiescence in the DG. This increase in YFP+ cell proliferation could be rescued by replacement of a single allele of Rb (Figures S1B and S1C). To define the phenotype of YFP+ cells generated in Rb-TKO mice, we co-stained for YFP and Prox1, a marker for commitment to a granule cell neuron fate, and NeuN, a marker for mature neurons. Rb-TKO cells exhibited a 2.5-fold impairment in induction of Prox1 (Figure 1B), and absence of terminal neuronal differentiation (NeuN) (Figure 1C). Rb-TKO cells underwent cell death, evident by an 3.2-fold increase in the percentage of active caspase-3 (AC3) staining (Figure 1D; see actual numbers in Figure S1D). By 8 wpi, the entire adult NSC niche was depleted, exhibiting a 5.7-fold depletion of the Sox2+ population (Figure 1E). Co-labeling with YFP and S100B, a marker for astrocytes, revealed a significant 1.8-fold increase in S100B labeling in YFP+ recombined cells, consistent with the disposable stem cell model, where NSC terminal differentiation to an astrocytic lineage contributes to SGZ niche depletion (Encinas et al., 2011). These results demonstrate that Rb family proteins are essential for control of SGZ NSC quiescence and long-term niche maintenance.

Because the subventricular zone (SVZ) is another adult NSC niche with properties distinct from the SGZ, we wanted to determine whether the Rb family requirement was similar between niches. In the SVZ, there were 3.4-fold and 2.5-fold increases in proliferation in recombined (YFP+) cells at 4 and 8 weeks, respectively, resulting in expansion of the YFP+ population at 4 wpi in Rb-TKO. This includes a 1.9-fold increase in Dcx+ cells (Figure 1F) as well as a 2.7-fold relative expansion of recombined Nestin/GFAP radial glia-like cells at 4 wpi (Figure 1G). Although there was an expansion of Dcx+ cells, the proliferation rate of this population was similar to controls (Figure S2A), suggesting that this expansion is not due to Rb action on neuroblast cell cycling but in their production. The YFP+ cell numbers began to decline at 8 wpi, with a concomitant 39-fold increase in cell death (Figures 1G and S1D). Consistent with an impairment in differentiation, the Rb-TKO SVZ generated periventricular heterotopias (Figure S2B), characterized by accumulation of Dcx+ cells, which developed as a mass in the lateral ventricle, a structure observed in human disease (Ferland et al., 2009), whereas cultured NSCs continuously proliferate throughout induced differentiation (Figure S2C). Our results show that Rb family proteins play a critical role in control of cell division, survival, and differentiation in the SVZ neurogenic niche, but niche depletion was not evident by 8 weeks as seen in the SGZ.

To interrogate the mechanisms by which Rb family proteins control NSC fate, we isolated, by fluorescence-activated cell sorting (FACS), the recombined YFP+ cells directly from the SVZ of adult Rb-THC and Rb-TKO mice to define transcriptomic profiles 10 days post Tam. We used bulk RNA sequencing (RNA-seq) to ensure the necessary sequencing depth for differential expression analyses. Proportionally, the YFP+ fraction of Rb-TKO cells was 3-fold greater than Rb-THC (Figure 2A, quadrant 2 [Q2]), in line with SVZ characterization (Figure 1F). Efficient knockdown of Rb family proteins was confirmed (Figures 2B and S3A–S3C). Transcriptomics analysis identified 4,817 significantly differentially expressed genes (DEGs) with a DESeq2-adjusted p value of less than 0.05 (Figure 2C). The DEGs were broken down into signature themes, including cell cycle, genes associated with NSC quiescence, activation, differentiation, and signaling (Figure 2D). Loss of pRb/p107/p130 resulted in upregulation of genes associated with cell cycle activation (Cyclins A2, E2, Cdks1/2, thymidine kinase, Cdc6) and downregulation of genes associated with quiescence, including Aqp4, Id3, Pdgfrb, Aldoc, Fgfr3, and Dbi (Delgado et al., 2021; Urbán et al., 2019). In contrast, genes and signaling pathways associated with NSC activation were significantly induced, including Ezh2, Suz12, and Pcna, together with upregulation of activated NSC markers, including Nestin and Pax6 and the Shh, Wnt, and Jak2 pathways (Kim et al., 2017). Thus, Rb family proteins are not only required for cell cycle control but also for control of genes required to regulate the phenotypic signature of quiescent NSCs.

Because Rb family proteins function by regulating transcription through several factors, we next pursued the E2F family,

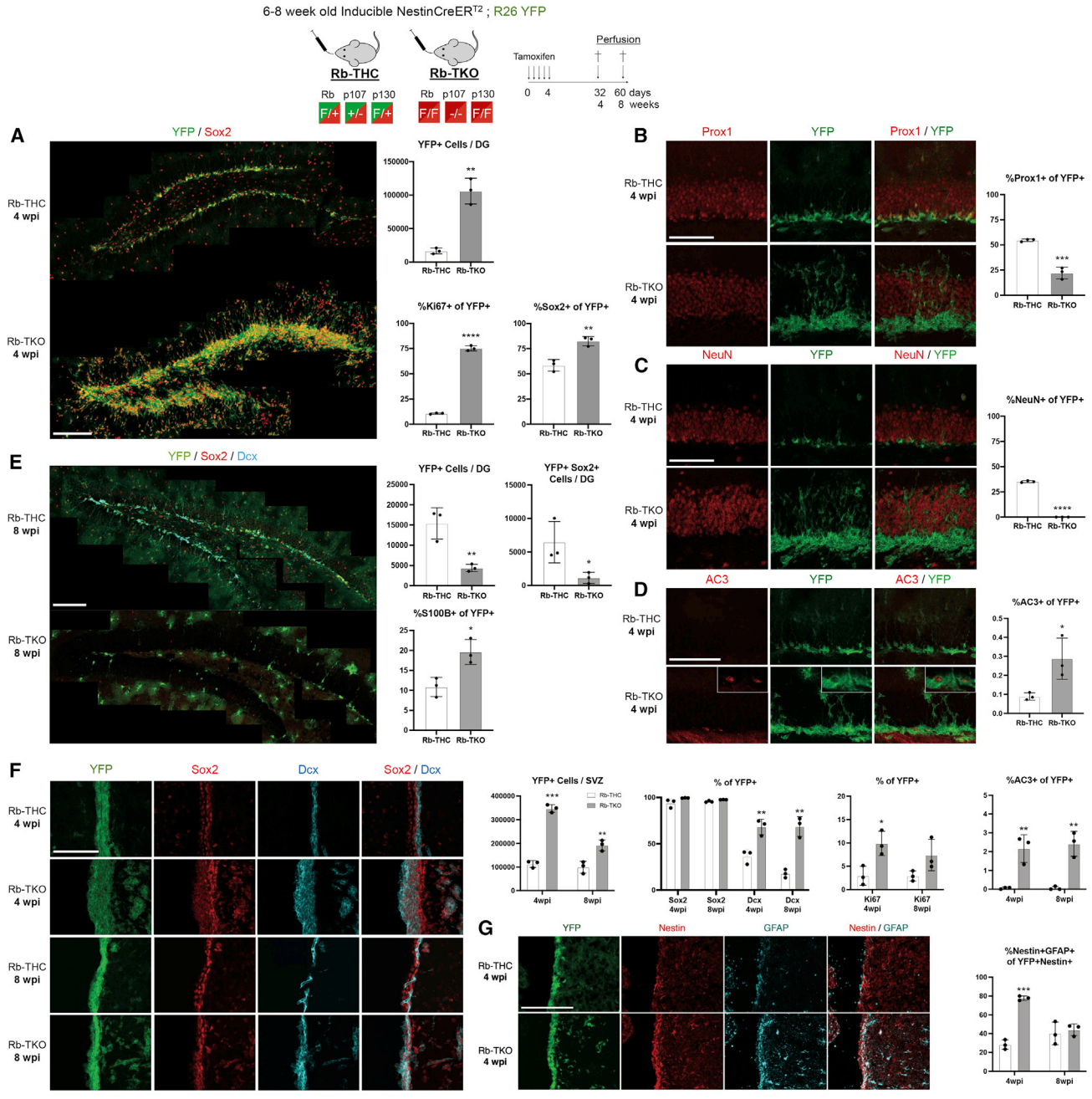

Figure 1. Rb family members are essential for regulation of adult NSC activation and quiescence

(A–G) IHC and quantification of cells in the DG (A–E) and SVZ (F and G) in genotypes are shown. (A) Total YFP+ recombined cells per DG, percentage of Sox2+, and percentage of Ki67+ cycling cells among YFP+ recombined cells. (B) Percentage of Prox1+ committed cells among YFP+ recombined cells. (C) Percentage of NeuN+ neurons among YFP+ recombined cells. (D) Percentage of AC3+ apoptotic cells of YFP + recombined cells. (E) Total YFP+ recombined cells per DG, total Sox2+/YFP+ cells per DG, and percentage of S100B+ astrocytes among YFP+ recombined cells. (F) Total YFP+ recombined cells per SVZ and percentage of Sox2, DCX, Ki67, and AC3 of YFP+ recombined cells in the SVZ. (G) Percentage of Nestin+/GFAP+ cells among YFP+ Nestin+ recombined cells.

Scale bars, 100 μm. Error bars, mean ± SD. Unpaired 2-tailed Student's t test; *p < 0.05, **p < 0.01, ***p < 0.001, ****p < 0.0001. n = 3 biological replicates.

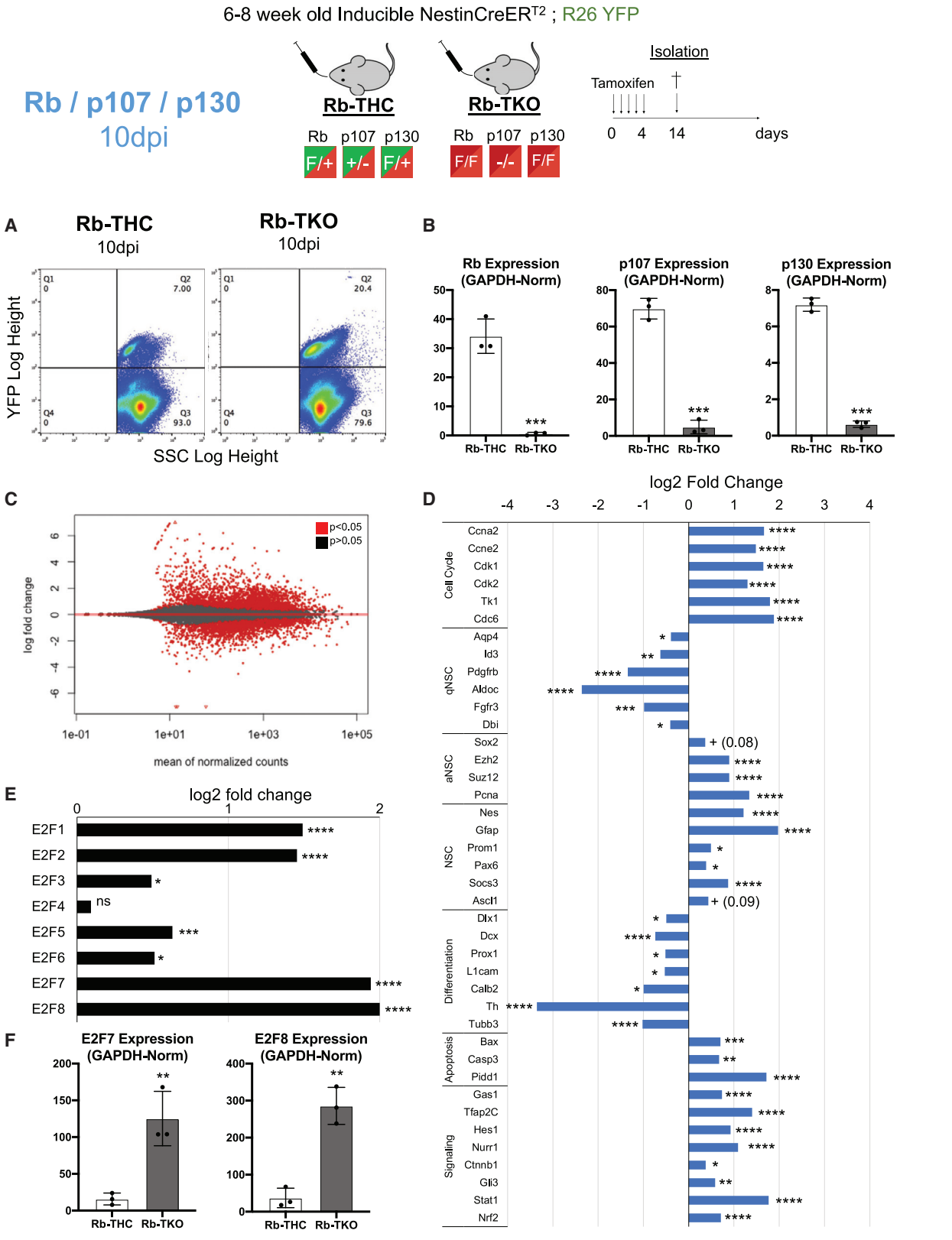

(legend on next page)

their best-known regulatory targets. RNA-seq reveals that activator E2F1/2/3, repressor E2F5/6, and atypical E2F7/8 were significantly upregulated in the absence of the Rb family (Figures 2E and 2F). Given that expression of activator E2Fs is significantly induced in the NSCs of Rb-TKO animals, and that E2F1 and E2F3 are highly expressed in this population (Callaghan et al., 1999), we wanted to determine whether Rb family proteins mediate their function through activator E2F1/3. We generated Tam-inducible NestinCreER^{T2};R26-eYFP mice to delete E2F3 together with germline deletion of E2F1 (E2F1/3-DKO), with mice double-heterozygous (E2F1/3-HET) as littermate controls. Recombined YFP+ cells were isolated by FACS directly from the SVZ of adult E2F1/3-HET and E2F1/3-DKO mice 10 days post Tam. We identified 4,514 significant DEGs with a DESeq2-adjusted p value of less than 0.05 (Figure 3A). Efficient knockdown of activator E2F1/3 was confirmed (Figures 3B and S3D–S3F). E2F1/3-DKO mice exhibited the opposite phenotype as that found in Rb-TKO mice because NSCs failed to undergo activation, showing cessation of adult neurogenesis (Figure 3C). Cell cycle genes were significantly downregulated, quiescence genes (Aqp4, Id3, Pdgfrb, Apoe, Fgfr3, and Dbi) were highly induced and validated (Figure 3D), and genes associated with NSC activation were downregulated. To confirm this deep quiescence phenotype, we examined the SGZ NSC niche of E2F1/3-DKO and E2F1/3 HET controls 4 and 8 wpi (Figures 3E and S3G). There was a striking impairment in NSC activation and cessation of neurogenesis, with a 15.2-fold decrease in Ki67+ cells and 11.8-fold decrease in Dcx+ neuroblasts at 4 weeks, which continued to decline at 8 weeks (Figure 3F). Loss of E2F1/3 resulted in a major reduction in Sox2+ cell proliferation in the SVZ and SGZ (Figures S3G and S3H). These data reveal a critical requirement for the activator E2Fs E2F1 and E2F3 to execute NSC activation.

We find that Rb-TKO and E2F1/3-DKO populations exhibit opposing regulation of gene transcripts associated with quiescence and activation signatures (Figures 4A, S4A, and S4B), whose coordinated function is critical to maintain the NSC niche. We compared each of our transcriptomic profiles with two published datasets, first a single-cell RNA-seq dataset with distinct clusters spanning all stages of adult SVZ neurogenesis (Basak et al., 2018). Rb-TKO populations exhibited striking upregulation of genes specific to activated NSC and progenitor cells, accompanied by simultaneous downregulation of quiescence-specific genes (Figure 4B). In contrast, loss of activator E2F1/3 resulted in upregulation of genes specific to quiescent NSCs and downregulation of genes associated with NSC activation (Figure 4D). The transcriptomes were then compared with datasets characterizing activated and quiescent NSC populations (Codega et al., 2014). In our Rb-TKO signature, 611 significant and majority-downregulated DEGs overlap with the quiescent NSC signature, and 478 significantly and majority-upregulated DEGs overlap with the activated NSC signature (Figure 4C). In the E2F1/3-DKO signature, 512 significant and vastly upregulated DEGs overlap with the quiescent NSC signature, and 553 significant and downregulated DEGs overlap with the activated NSC signature (Figure 4E). Alignment with published datasets suggests important roles of Rb family proteins and activator E2F1/3 in regulation of the molecular signatures associated with NSC quiescence and activation.

To uncover the mechanisms underlying Rb-E2F-mediated regulation of NSC fate, we searched for master transcriptional regulators and key pathways controlled by the Rb/E2F axis (Figure 5A). We used iRegulon to establish the enrichment of transcription factor motifs surrounding the transcriptional start sites of significantly downregulated genes. We found consistent evidence in Rb-TKO and E2F1/3-DKO, supporting a role of the Rb/E2F axis as an upstream regulator of REST, the RE1-silencing transcription factor, a transcriptional repressor (Chong et al., 1995; Schoenherr and Anderson, 1995) known to control neuron-specific gene promoters (Mu et al., 2012). Studies have demonstrated a requirement for REST in maintaining adult NSC quiescence in the SVZ and SGZ (Gao et al., 2011; Mukherjee et al., 2016; Soldati et al., 2015). The Rb-TKO dataset revealed REST-regulated RE1 motifs on 738 gene targets (31% of input) as well as motifs corresponding to the known REST target Sox11 (Bergsland et al., 2006) on 151 gene targets (6% of input). Similarly, the E2F1/3-DKO dataset revealed RE1 and Sox11 motifs on 76 and 603 gene targets (representing 3% and 28% of input), respectively. We used Network Analyst to construct a molecular network and compare significant DEG targets with the ENCODE transcription factor-gene interactions database. For both datasets, the REST cofactors SIN3A and CoREST (Rcor1) were significantly interconnected with the DEGs. This is supported by significant upregulation of REST in either dataset, accompanied by significant downregulation of the REST targets Sox4 and Sox11 (Figure 5B). Dysregulation of REST, REST cofactors, and downstream regulatory targets suggests that the Rb/E2F axis may regulate REST function.

To determine whether REST is regulated by the Rb/E2F axis, we first wanted to determine whether endogenous REST protein was altered in the absence of Rb family proteins. FACS-isolated SVZ NSCs from Rb-THC and Rb-TKO mice, 10 days post Tam, were cultured, and early differentiation was evaluated over a time course of 3 days. In Rb-THC NSCs, western blots revealed that REST expression decreases within 1 day of differentiation, consistent with previous findings (Ballas et al., 2005; McGann

Figure 2. Transcriptomic analysis of Rb family function in the neurogenic niche

(A) Representative 488FL-log height versus SSC-log height FACS plots demonstrating the gating strategy. The YFP+ enriched population is defined in Q2.

(B) qPCR analysis of Rb, p107, and p130 mRNA, normalized to GAPDH.

(C) MA plot for the shrunken $\log_2$ fold changes. Significant DEGs ($p < 0.05$) are indicated in red.

(D) Relative expression of significant DEGs, grouped by curated functional category.

(E) Relative expression of E2F family transcription factors.

(F) qPCR of E2F7 and E2F8, normalized to GAPDH.

Error bars, mean ± SD. qPCR analysis (B and F), unpaired 2-tailed Student's t test; relative expression plots (D and E), DESeq2-adjusted p value. *$p < 0.05$, **$p < 0.01$, ***$p < 0.001$, ****$p < 0.0001$. n = 3 biological replicates.

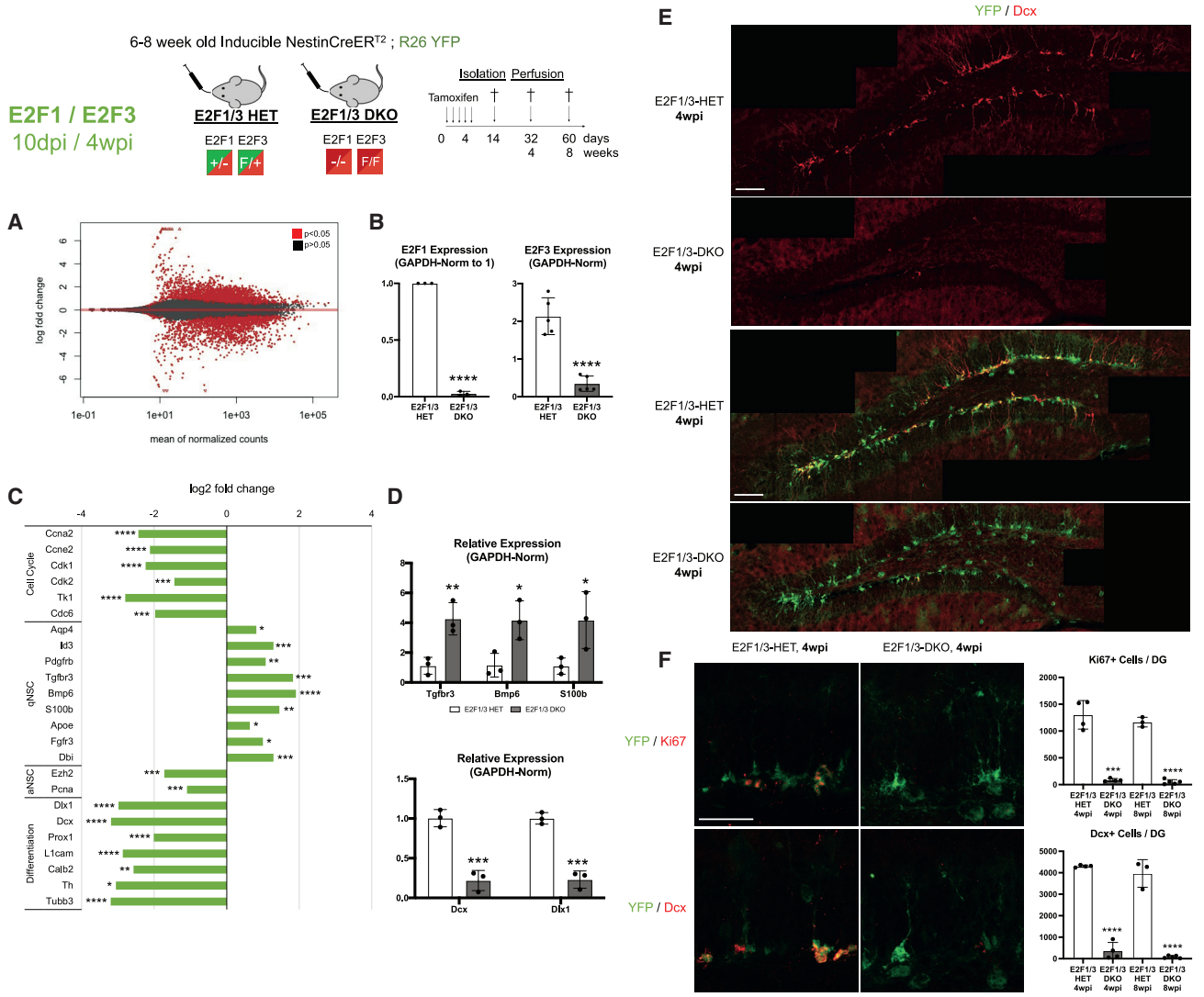

Figure 3. Activator E2Fs 1 and 3 are essential for adult NSC activation and neurogenesis

(A) MA plot for the shrunken log2 fold changes. Significant DEGs ($p < 0.05$) are shown in red.

(B) qPCR of E2F1 and E2F3 mRNA, GAPDH normalized to 1 following the $2^{-\Delta\Delta Ct}$ method.

(C) Relative expression of significant DEGs, grouped by curated functional category.

(D) qPCR of the quiescence-associated genes Tgfbr3, Bmp6, and S100β and differentiation-associated genes Dcx and Dlx1. Values were GAPDH normalized to 1 following the $2^{-\Delta\Delta Ct}$ method.

(E) IHC of YFP+ recombined cells and DCX+ neuroblasts (red) in the DG. Scale bars, 100 μm.

(F) IHC and quantification of total YFP+ recombined cells, total Ki67+ cycling cells, and total Dcx+ neuroblasts in the DG at 4 and 8 wpi.

Error bars, mean ± SD. IHC and qPCR analysis (B, D, and F), unpaired 2-tailed Student's t test; relative expression plot (C), DESeq2-adjusted p values. *$p < 0.05$, **$p < 0.01$, ***$p < 0.001$, ****$p < 0.0001$. n = 3 biological replicates (A–D); n = 5 biological replicates (E and F).

et al., 2020). In contrast, REST remains highly expressed in Rb-TKO NSCs induced to differentiation (Figure 6A). To determine whether the Rb family proteins and activator E2Fs may regulate REST expression, we first searched for E2F consensus sites at REST regulatory regions and identified 5 motifs within REST introns/exons (Figure 6B). Using chromatin immunoprecipitation (ChIP), we found significant binding by p107, p130, E2F3, and E2F4 at motifs in close proximity: 1 (bs1) and 2 and 3 (bs2/3) (Figure 6C). Significant E2F1 binding was found at bs2/3 (Figure 6D). The identified binding at REST was significant compared with immunoglobulin G (IgG) and negative locus control Cacng1 (Figures 6C and 6D). p107, p130, E2F3, and E2F binding was confirmed with p107-deficient and Rb-TKO NSCs (Figures 6C, 6D, S5A, and S5B). Binding at Ccna2 (Figure S5C) was used as positive target of Rb family proteins and E2Fs (Julian et al., 2016; Litovchick et al., 2007). These results identify binding of Rb/E2F proteins within REST regulatory regions and suggest a requirement for Rb family proteins in regulation of REST in NSCs.

To determine whether dysregulation of REST contributes to the Rb-TKO NSC phenotype, we examined the expression of

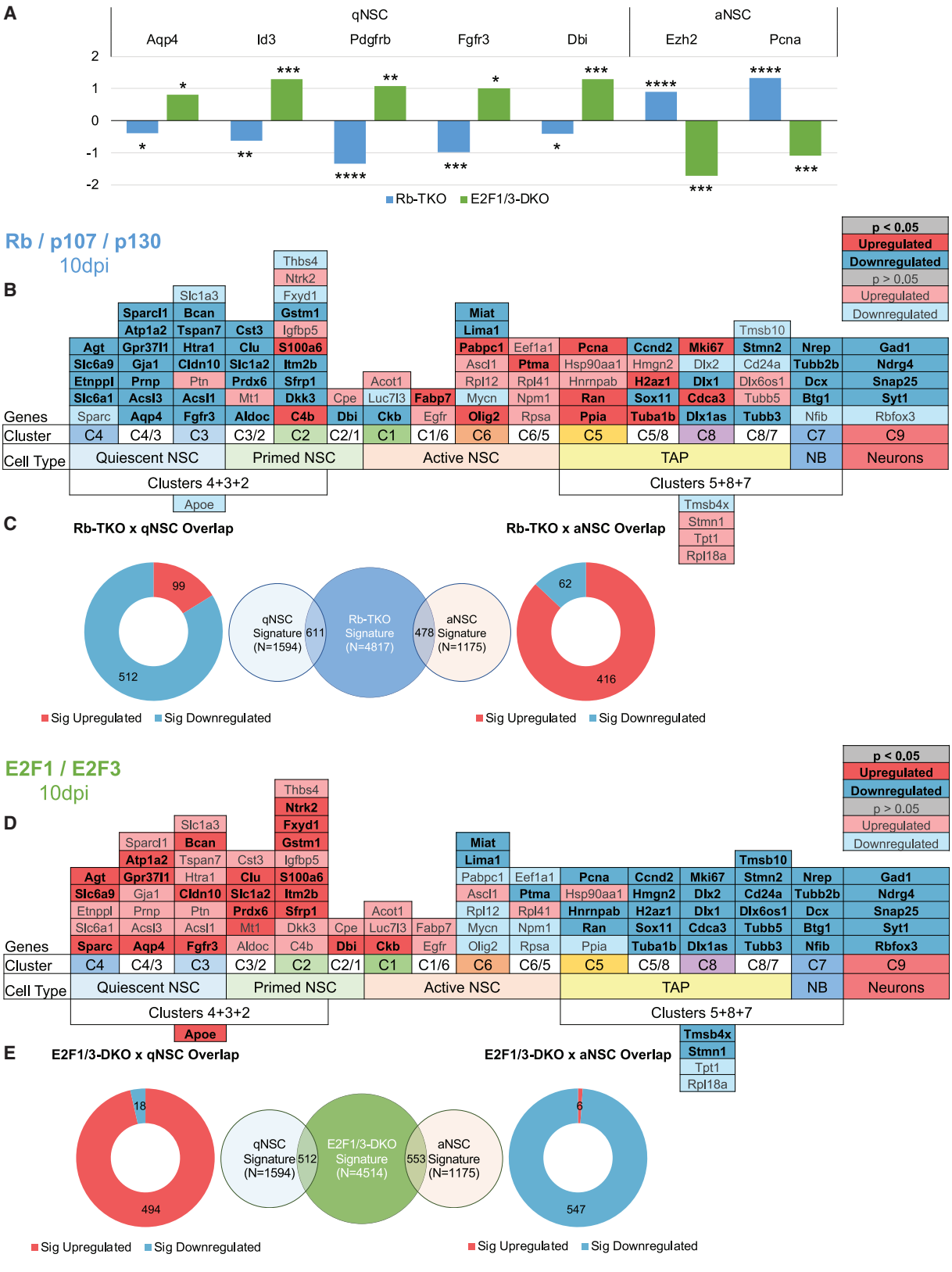

(legend on next page)

neuronal differentiation markers by western blot (Figure 6E). In Rb-TKO NSCs, expression of the neuroblast markers Dcx and βIII-tubulin was impaired, whereas the pro-activation factor ASCL1 was elevated (Figures 6E and 6F). To determine whether dominant-negative REST (dnREST) could rescue the phenotype of Rb-TKO NSCs, cells were transduced with lentivectors expressing dnREST-V5-mCherry (Chong et al., 1995) or an mCherry control. Although dnREST-V5 was not able to rescue expression of differentiation markers in Rb-TKO NSCs, it resulted in a significant increase in ASCL1 expression (Figures 6E and 6F). These results suggest a requirement for the Rb/E2F pathway in repressing REST activity to enable expression of REST target genes, including ASCL1.

Recent studies have defined a dynamic role of ASCL1 in regulation of activation and quiescence because ASCL1 is localized to activated NSCs in the SVZ and SGZ, becoming induced upon activation (Andersen et al., 2014) and eliminated upon reentry into quiescence through HUWE1-mediated degradation (Urbán et al., 2016). Using immunohistochemistry in the SGZ, we observed strong upregulation of ASCL1 in response to Rb-TKO (Figure 7A), reflecting a 2.1-fold increase in the proportion of recombined cells expressing ASCL1. Performing ChIP against an E2F site at the ASCL1 promoter we reported previously in embryonic NSCs (Julian et al., 2016) revealed E2F3, E2F4, p107, and p130 binding in wild-type adult NSCs differentiated for 0 or 1 days (Figure 7B), with the Ccna2 promoter used as a positive control (Figure S5C). These results reveal consistently elevated ASCL1 expression in the absence of Rb family proteins, suggesting that the Rb/E2F axis plays an important role in regulation of ASCL1.

Given the increase in ASCL1 expression in response to dnREST-V5 (Figures 6E and 6F), we next wanted to determine whether Rb/E2F regulation of ASCL1 may be influenced by REST. Although previous studies revealed regulation via an RE-1 site 49 kb downstream of ASCL1 (Ballas et al., 2005; Jørgensen et al., 2009), we uncovered REST binding at a distinct peak 94 kb upstream of ASCL1 (Figures S6A–S6C), with REST being the regulated gene closest to this peak (Figures S6D and S6E). ChIP in wild-type adult NSCs differentiated for up to 3 days confirms significant binding of REST at the 94-kb peak alone, increasing with differentiation time, with Snap25 used as a positive REST target (Figure 7C). These results show that the Rb/E2F axis plays an important role in regulation of REST and ASCL1, with additional functional interaction on ASCL1 by REST.

Because REST and its regulatory network play a critical role in control of adult NSC quiescence and onset of differentiation, we examined the functional consequence of REST dysregulation by performing rescue experiments in the SGZ niche. At two wpi, we performed dual stereotaxic injections of lentivectors into both hemispheres, carrying dnREST-V5-mCherry or the mCherry control, targeting the DG of Rb-THC and Rb-TKO mice, respectively. We first wanted to determine whether dnREST could rescue expression of the REST target gene ASCL1 by measuring the proportion of ASCL1+YFP+ expression in mCherry-transduced cells at 4 and 14 dpi (Figures 7D, S7A, and S7B). 4 days after injection, there was a 2.8-fold increase in the proportion of ASCL1+ YFP+ cells in Rb-TKO in response to dnREST-V5, suggesting that dnREST results in an early increase in ASCL1 expression in NSCs. This increase in ASCL1+YFP + expression was also maintained 14 days after injection in Rb-TKO mice, suggesting that dnREST increases expression of ASCL1 in NSCs of Rb-TKO animals.

To determine whether dysregulated REST contributes to exhaustion of adult NSCs in Rb-TKO animals, we tested whether dnREST could rescue NSC depletion at 14 dpi (Figure 7E). Although transduction of Rb-THC controls with mCherry or dnREST-V5 had no effect on NSC maintenance after 14 days (Figure S7B), dnREST resulted in partial rescue of mCherry+ YFP+ expressing cells in Rb-TKO. Although double-labeled cells were readily detected at 4 days in Rb-TKO animals (Figure S7A), by 14 days there was a 14.6-fold depletion of LV-mCherry-transduced cells. Transduction of NSCs with dnREST-V5 resulted in a reduction in the number of apoptotic cells (AC3+ cells), consistent with partial rescue (only 3.8-fold depletion) of Rb-TKO double-labeled cells at 14 days (Figures 7E, S7C, and S7D). Thus, dnREST can partially rescue NSC depletion in Rb-TKO NSCs, showing that the Rb/E2F axis is required for proper regulation of REST, which is important for long-term maintenance of the adult NSC population.

The Rb/E2F axis regulates NSC function through coordination of cell cycle control with the transcriptional networks instructing phenotypes of adult NSC quiescence and activation, an important function for long-term maintenance of NSC and neurogenesis throughout life.

DISCUSSION

The results of these studies support a number of conclusions. First, we show that Rb family proteins are required for long-term maintenance of the adult NSC pool by playing an essential role in regulating NSC quiescence and activation, preventing niche depletion in the SGZ. Second, we show that activator E2F1/3 are critical Rb family regulatory targets that are essential for NSC activation because, in their absence, adult NSCs fail to become activated, and neurogenesis cannot proceed. Third, we show that the Rb/E2F axis is not only important for cell cycle control but also for induction of genes associated with the activation

Figure 4. Rb/E2F pathway transcriptomic regulation of NSC activation and quiescence

(A) Relative expression of significant qNSC-associated and aNSC-associated DEGs across both datasets.

(B) DEGs in response to Rb-TKO, including direction and significance, overlapped with the Basak et al. (2018) signature.

(C) Significant DEGs in response to Rb-TKO, overlapped with qNSC and aNSC signatures from (Codega et al., 2014), and proportional directionality of overlap.

(D) DEGs in response to E2F1/3-DKO, including direction and significance, overlapped with the Basak et al. (2018) signature.

(E) Significant DEGs in E2F1/3-DKO, overlapped with qNSC and aNSC signatures from (Codega et al., 2014), and proportional directionality of overlap.

Relative expression plot, DESeq2-adjusted p values. Genes with DESeq2-adjusted $p < 0.05$ were used as input for the respective signatures in (B) and (D) and (C) and (E). *$p < 0.05$, **$p < 0.01$, ***$p < 0.001$, ****$p < 0.0001$. n = 3 biological replicates.

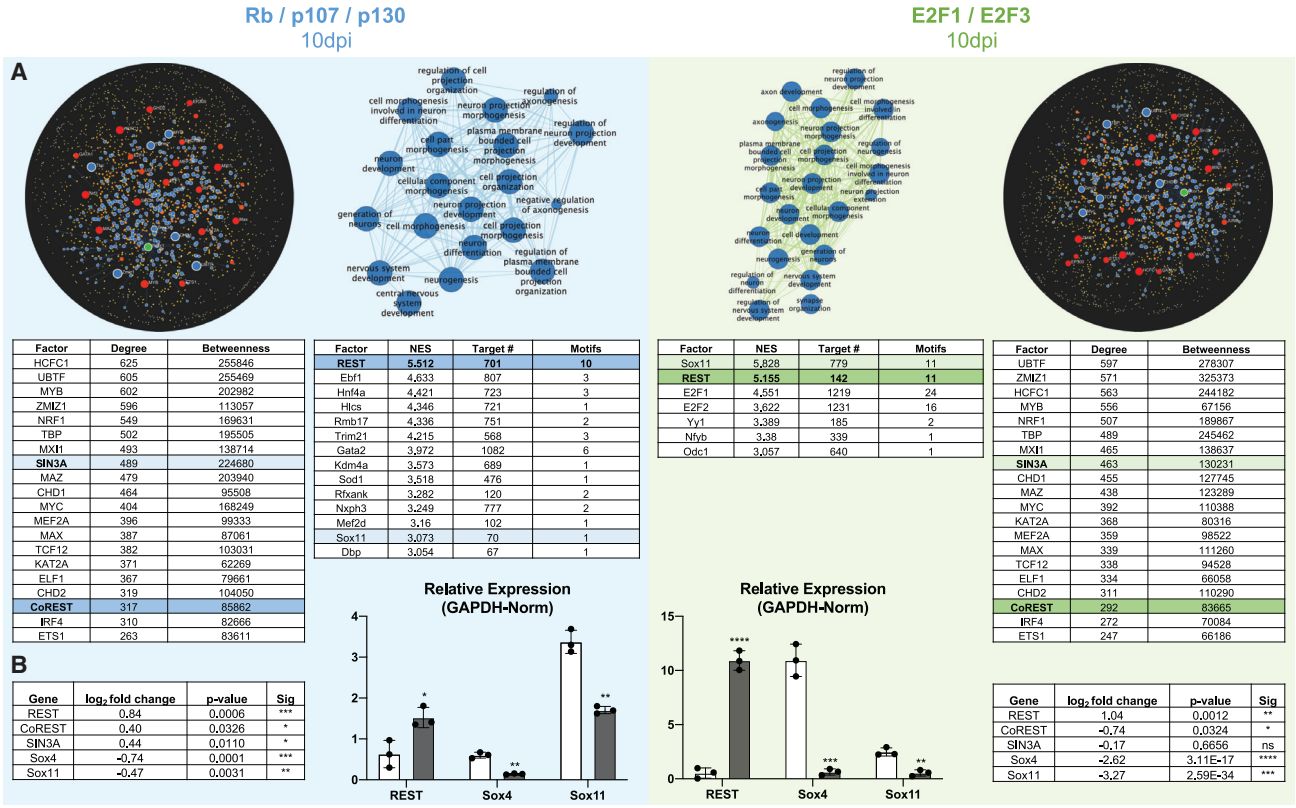

Factor	Degree	Betweenness
HCFC1	625	255846
UBTF	605	255469
MYB	602	202982
ZMIZ1	596	113057
NRF1	549	169631
TBP	502	195505
MXI1	493	138714
SIN3A	489	224680
MAZ	479	203940
CHD1	464	95508
MYC	404	168249
MEF2A	396	99333
MAX	387	87061
TCF12	382	103031
KAT2A	371	62269
ELF1	367	79661
CHD2	319	104050
CoREST	317	85862
IRF4	310	82666
ETS1	263	83611

Factor	NES	Target #	Motifs
REST	5.512	701	10
Ebf1	4,633	807	3
Hnf4a	4,421	723	3
Hlcs	4,346	721	1
Rmb17	4,336	751	2
Trim21	4,215	568	3
Gata2	3,972	1082	6
Kdm4a	3,573	689	1
Sod1	3,518	476	1
Rfxank	3,282	120	2
Nxph3	3,249	777	2
Mef2d	3,16	102	1
Sox11	3,073	70	1
Dbp	3,054	67	1

Gene	log_2 fold change	p-value	Sig
REST	0.84	0.0006	***
CoREST	0.40	0.0326	*
SIN3A	0.44	0.0110	*
Sox4	-0.74	0.0001	***
Sox11	-0.47	0.0031	**

Factor	NES	Target #	Motifs
Sox11	5.828	779	11
REST	5.155	142	11
E2F1	4.551	1219	24
E2F2	3.622	1231	16
Yy1	3.389	185	2
Nfyb	3.38	339	1
Odc1	3.057	640	1

Factor	Degree	Betweenness
UBTF	597	278307
ZMIZ1	571	325373
HCFC1	563	244182
MYB	556	67156
NRF1	507	189867
TBP	489	245462
MXI1	465	138637
SIN3A	463	130231
CHD1	455	127745
MAZ	438	123289
MYC	392	110388
KAT2A	368	80316
MEF2A	359	98522
MAX	339	111260
TCF12	338	94528
ELF1	334	66058
CHD2	311	110290
CoREST	292	83665
IRF4	272	70084
ETS1	247	66186

Gene	log_2 fold change	p-value	Sig
REST	1.04	0.0012	**
CoREST	-0.74	0.0324	*
SIN3A	-0.17	0.6656	ns
Sox4	-2.62	3.11E-17	****
Sox11	-3.27	2.59E-34	***

Figure 5. The Rb/E2F pathway regulates NSC fate via REST

(A) Medial: curated significant GO:BP gene sets using downregulated genes (in response to knockout) as input and iRegulon transcription factor enrichment results, using significantly downregulated genes as input. REST and Sox11 are highlighted in each. Lateral: Network Analyst TF-protein enrichment results, using all significant genes as input. The REST cofactors SIN3A and CoREST are highlighted in each.

(B) Lateral: summary of significant DEGs affecting the REST/SoxC pathway. Medial: qPCR of REST and SoxC, Sox4, and Sox11 normalized to GAPDH.

Error bars, mean ± SD. qPCR analysis (B), 2-tailed Student's t test; summary table, DESeq2-adjusted p values. Genes with DESeq2-adjusted $p < 0.05$ were considered significant for analysis using iRegulon and Network Analyst in (A). *$p < 0.05$, **$p < 0.01$, ***$p < 0.001$, ****$p < 0.0001$. n = 3 biological replicates.

and quiescence molecular signature. Fourth, Rb/E2F controls entry and exit from quiescence through regulation of key transcription factors, including REST and ASCL1. The Rb/E2F axis serves as an important regulator that coordinates cell cycle control with the molecular signature associated with the activation/quiescence phenotype, a function that is essential for long-term maintenance of adult NSCs and neurogenesis.

Rb family proteins are essential for adult NSC maintenance

Earlier studies by our group and others have shown that Rb is dispensable for adult NSC function in the SVZ and SGZ (Jaafar et al., 2016; Vandenbosch et al., 2016), whereas p107 is required for balancing self-renewal versus differentiation mediated through Hes1 (Vanderluit et al., 2004, 2007). Here we show that loss of all Rb family proteins results in loss of quiescence and activation of the adult NSC pool, playing a crucial role in regulating the function of adult NSCs. Although studies in other systems have established ectopic proliferation after Rb family deletion (Jiang et al., 2010; Sage, 2000; Viatour et al., 2008, 2011), functional compensation between Rb family proteins (Ajioka et al., 2007; Burkhart et al., 2010; Sage et al., 2003), and promotion of reprogramming after Rb inactivation (Kareta et al., 2015), the effect on the adult NSC population is dramatic because Rb family proteins regulate not only cell cycle control but the molecular signature associated with NSC quiescence and activation. Thus, the global changes identified in Rb-TKO signify an important role of Rb family proteins as broad transcriptional regulators of NSC fate.

Our data suggest that NSC activation in the Rb-TKO is a cell-autonomous phenomenon that results from the absence of pRb/p107/p130 pocket proteins. First, we have shown previously that inducible knockout of Rb only is not compatible with neuronal survival in the embryo or the adult hippocampus (Vandenbosch et al., 2016); however; we did not observe any activation (i.e., more proliferation) of Sox2 NSCs after neuronal cell death. Second, in Figure S1C we show that expansion of the NSC pool occurs very early after TKO induction (10 dpi), also suggesting that NSC activation is a direct consequence of Rb/p107/p130 loss. However, previous evidence suggests that loss of Tbr2+ intermediate progenitors (Hodge et al., 2012) or loss of neuroblasts and neurons after hypoxic-ischemic injury or traumatic brain injury may also contribute to adult NSC activation (Miles and Kernie, 2008; Wang et al., 2016). Given that significant progenitor

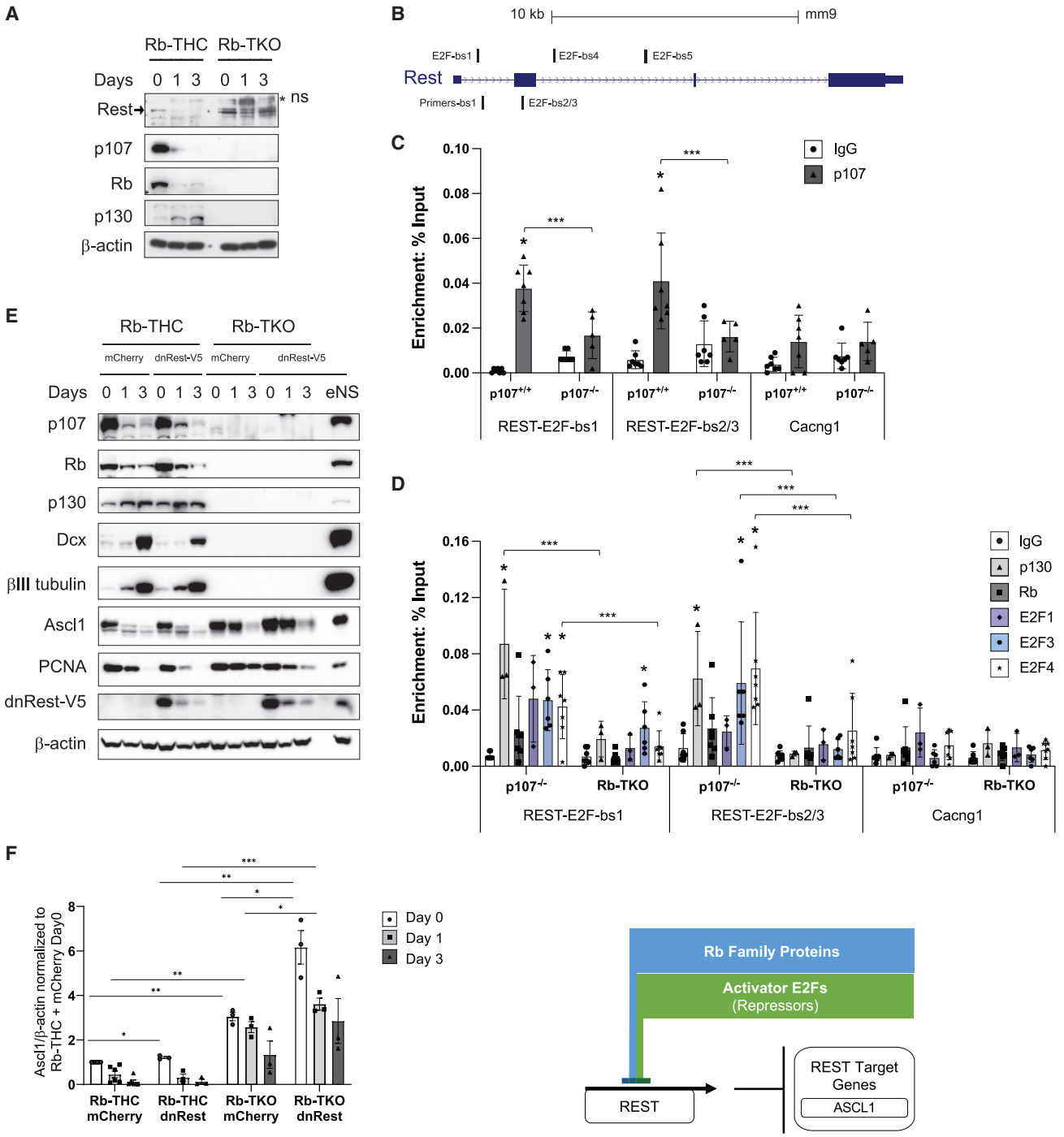

Figure 6. Rb family proteins regulate REST expression in adult NSCs

(A) Western blot (WB) of total protein from NSCs differentiated for 0, 1, or 3 days; β-actin is the loading control.

(B) Schematic of the REST gene, indicating the presence of 5 E2F motifs.

(C) ChIP of NSC chromatin from wild-type +/+ and p107-null −/− mice. Error bars, mean ± SEM.

(D) ChIP of p107-null −/− NSCs and Rb-TKO NSCs. Error bars, mean ± SEM.

(E) WB from NSCs infected with LV-mCherry or dnREST-V5 at post-natal day 2 (P2) and differentiated at P3 for 0, 1, or 3 days. eNS, embryonic neurospheres to test LV expression vectors.

(legend continued on next page)

and neuroblast loss occurs in the Rb-TKO, we cannot rule out that a proportion of the NSC activation found in these animals is, at least in part, indirectly due to loss of progenitors and neuroblasts, contributing to the widespread NSC activation.

The activator E2Fs E2F1 and E2F3 are essential for NSC activation

Rb family proteins are known to associate with at least 110 regulatory targets that modulate transcription (Morris and Dyson, 2001), with the best-characterized being E2F family transcription factors: the activators E2F1–E2F3a and repressors E2F3b–E2F6. Here we show that E2F1 and E2F3 are critical for NSC function because absence of both of these factors results in complete cessation of NSC activation and neurogenesis. Previous studies have demonstrated a moderate decrease in adult NSC proliferation (Cooper-Kuhn et al., 2002), and we have shown that loss of E2F3 or the individual isoforms E2F3a or E2F3b results in imbalances in self-renewal/commitment decisions (Julian et al., 2013; McClellan et al., 2007). None of the phenotypes reported previously with individual E2Fs have resulted in the dramatic phenotypes generated by loss of E2Fs1/3, where adult NSCs are unable to exit quiescence. Earlier studies revealed that retinal progenitors and activated Müller glia can proliferate in the absence of activator E2F1/2/3, unlike what is seen in the adult neurogenic niches described here (Chen et al., 2009). Thus, our results demonstrate that activator E2F1/3 are essential for adult NSC activation and for generation of the molecular signature required for NSC activation and neurogenesis.

The Rb/E2F axis regulates phenotypes of adult NSC quiescence and activation

These results highlight a function for the Rb/E2F axis, revealing a critical requirement not only for cell cycle control but for acquisition of the cell and transcriptomic phenotypes associated with quiescence and activation. Recent studies have demonstrated that quiescence is an active, dynamic process where NSCs progressing between states of quiescence and activation possess distinct gene expression profiles that allow quiescent NSCs to respond to environmental cues, ultimately culminating in NSC activation (Basak et al., 2018; Codega et al., 2014) Alignment of our transcriptomic profiles with published population-specific signatures reveals a striking alignment where loss of Rb family proteins aligns with an activated state, and loss of E2Fs1/3 aligns with the molecular signature of the quiescent state. The depth of cell quiescence and reduced sensitivity to growth signals reflected in these signatures has yet to be evaluated; previous studies have suggested that quiescence depth may be associated with an increased threshold required to activate an Rb/E2F switch (Kwon et al., 2017). We show that the Rb/E2F axis not only controls the cell cycle in NSCs but also plays an important role in generating the molecular signature of quiescent and activated cells.

The Rb/E2F axis regulates NSC fate via REST

Our transcriptomic profiles suggest an Rb/E2F-dependent mechanism regulating the molecular signatures of NSC quiescence and activation. After loss of Rb family proteins or activator E2Fs, we observe dysregulation of the REST gene regulatory network, with elevated REST and downregulation of numerous proneural targets containing RE-1 sites, including Dcx, L1cam, and the SoxC proteins Sox4/Sox11 (Bergsland et al., 2006; Lepagnol-Bestel et al., 2009; Mu et al., 2012). REST has been shown recently to maintain NSC quiescence as well as progenitor proliferation and numbers to prevent precocious differentiation (Mukherjee et al., 2016). Given that Rb-TKO and E2F1/3-DKO generate opposing phenotypes in regulation of NSC quiescence and activation, the common induction of REST and its targets may appear contradictory. Although activator E2Fs can function as transcriptional activators in proliferating cells, they have also been shown to serve as transcriptional repressors to silence E2F target genes in differentiating cells, so that activating E2Fs serve as a tether to recruit Rb family proteins to target genes (Chong et al., 2009). In the context of the adult neurogenic niche, our data suggest that activator E2F1/3 are essential for Rb family-mediated repression of REST. Analysis of transcriptomics and ChIP data demonstrate binding by p107/p130 and E2F3/E2F4 at the REST regulatory regions, consistent with a model where E2F1/3 recruit Rb family proteins to repress REST in adult NSCs. The increased magnitude of REST target gene repression in response to E2F1/3 deficiency is consistent with activator E2Fs mediating Rb family protein function to regulate REST. In response to E2F1/3-DKO, the lack of REST cofactor (CoREST and Sin3A) upregulation suggests that activator E2Fs are required to recruit REST cofactors. This may link activator E2Fs with a reported requirement for CoREST in modulating REST target expression despite REST dissociation (Ballas et al., 2005). Based on this model, we show that Rb family proteins and activator E2F1/3 together are required for REST regulation.

The Rb/E2F axis and REST are required for ASCL1 regulation

In response to loss of Rb family proteins, we observe that the transcriptional shift toward activation is accompanied by an increased number of ASCL1-expressing activated NSCs. Together with ChIP data demonstrating direct ASCL1 binding by p107/p130 and E2F3/E2F4, our data suggest a role of the Rb/E2F axis in repressing ASCL1 expression to maintain NSC quiescence. Although ASCL1 regulation occurs at multiple levels, most notably at the level of protein degradation mediated by the E3 ubiquitin ligase Huwei1 (Urbán et al., 2016), we also demonstrate that dnREST transduction results in increased ASCL1 expression, consistent with ASCL1 being a regulatory target for REST (Gao et al., 2011). Distinct from a previously described site (Ballas et al., 2005; Jørgensen et al., 2009), in the context of adult NSCs, we identified REST binding at a distinct peak 94 kb upstream of ASCL1. REST regulation of

(F) Quantification of the WB in (E) using ImageJ.

WB analysis (F): paired 2-tailed Student's t test; *p < 0.05, **p < 0.01, ***p < 0.001, n = 3–6. ChIP analysis: unpaired 2-tailed Student's t test; *p < 0.05 versus IgG and Cacng1, ***p < 0.05 in wild-type (WT) versus p107-null (C) or p107-null versus Rb-TKO mice (D). n = 3–7 biological replicates; cell culture, 3 technical replicates.

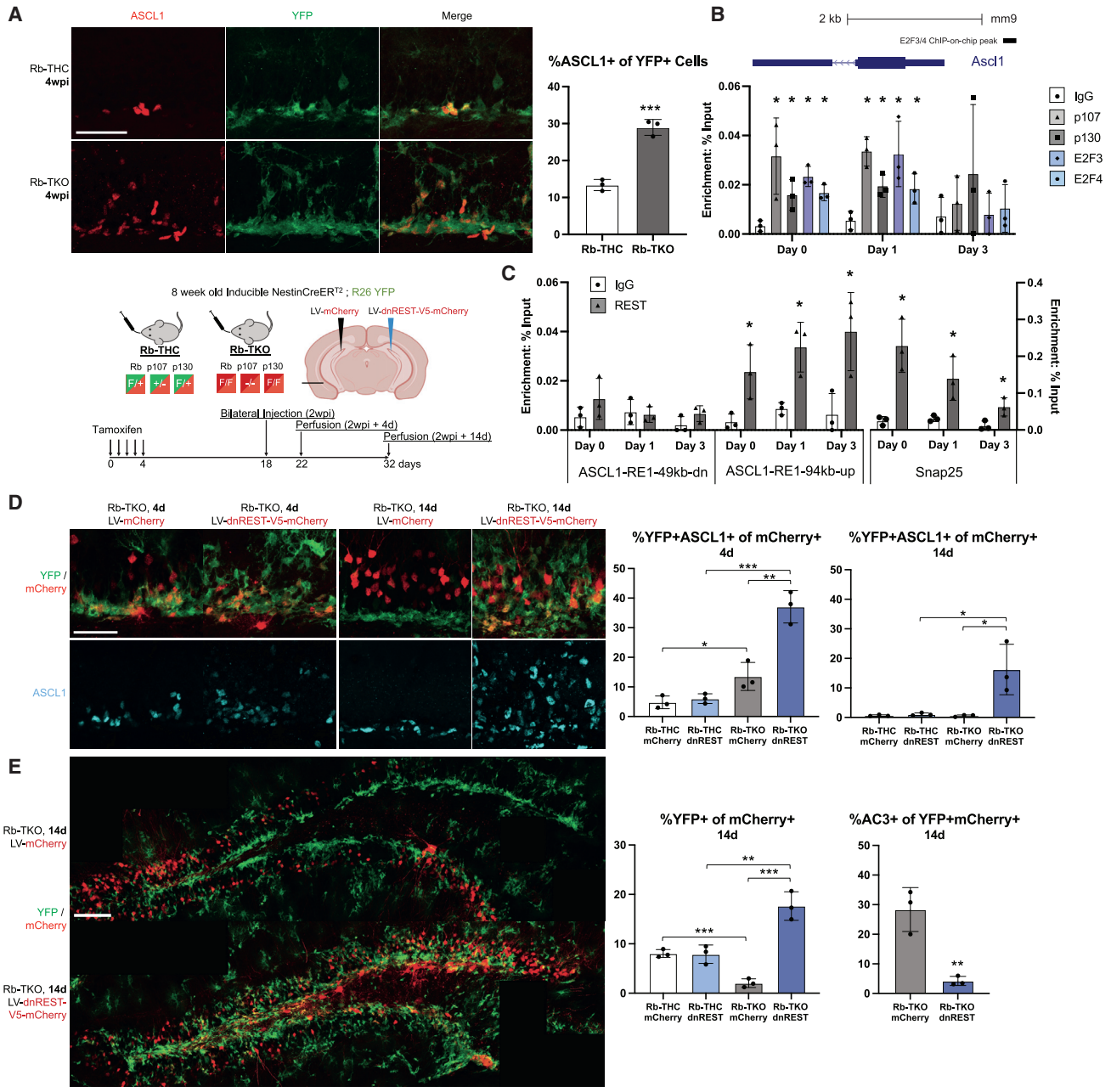

Figure 7. The Rb-E2F pathway regulates NSC activation and quiescence through REST and ASCL1

(A) IHC staining of ASCL1+ and YFP+ recombined cells in the DG. Scale bar, 50 μm. Quantification of the percentage of YFP+ ASCL1+ among YFP+ recombined cells.
(B) Schematic of the ASCL1 gene, indicating the E2F3/4 peak at the promoter (Julian et al., 2016), and ChIP of NSC chromatin from WT +/+ mice, differentiated for 0, 1, or 3 days, targeting this peak.
(C) ChIP of NSC chromatin from WT +/+ mice, differentiated for 0, 1, or 3 days, targeting the specified peak.
(D) IHC staining and quantification of ASCL1+/YFP+ recombined cells among total mCherry+ cells at the indicated time points.
(E) IHC staining and quantification of the percentage of YFP+ among total mCherry+ cells 14 days after injection and percentage of AC3+ apoptotic cells among total mCherry+/YFP+ recombined cells. Scale bar, 100 μm.
Error bars, mean ± SD. Unpaired 2-tailed Student's t test. ChIP analysis (B and C): *p < 0.05 versus IgG. n = 3 biological replicates, 3 technical replicates. IHC (A, D, and E): *p < 0.05, **p < 0.01, ***p < 0.001, ****p < 0.0001. n = 3 biological replicates.

ASCL1 is also supported by our findings *in vivo* because dnREST transduction results in an increased percentage of ASCL1-expressing cells in the adult SGZ. dnREST partially rescued depletion of adult NSCs after loss of Rb family proteins because dnREST resulted in a significant increase in Ascl1-expressing cells after 14 days. This suggests that the Rb/E2F regulatory

axis is required for proper REST regulation, which is important for maintenance of the NSC niche in the adult SGZ.

Limitations of the study

Here, we describe an important role of the Rb-E2F axis in regulating adult NSC function in the two adult neurogenic niches, but it is important to note that the SVZ and SGZ function in different ways. We used the Nestin promoter to drive Cre, but, contrary to SGZ, where Nestin is expressed in activated NSCs (aNSCs) and quiescent NSCs (qNSCs), in the SVZ, Nestin expression is restricted to aNSCs and ependymal cells (Codega et al., 2014). Thus, in the SVZ, we can determine the function of Rb-E2F on aNSCs themselves and not on the switch between qNSCs and aNSCs. A portion of the aNSCs in the SVZ and SGZ return to quiescence after activation to maintain the NSC pool, as reviewed previously (Obernier and Alvarez-Buylla, 2019; Urbán et al., 2019). Thus, our data reveal a critical requirement for RB Proteins in the Rb TKO SVZ to enable re-entry of adult aNSCs into quiescence. Our E2F1/3 DKO data, using the same Nestin-CreERT2, support a role of the Rb/E2F pathway in regulation of NSC activation/quiescence because we observe an impairment of NSC activation *in vivo* in the SGZ and SVZ, along with a transcriptional signature toward quiescence in aNSCs from the SVZ. Thus, targeting aNSCs, a cycling population that is expressing high levels of activator E2Fs, drives aNSCs to re-enter a qNSC-like state. Finally, based on the phenotypic data obtained in the SGZ of Rb TKO and E2F1/3 DKO, we postulate that the mechanisms highlighted in our study may be extrapolated to the qNSC-to-aNSC switch. Further transcriptomics studies using Cre drivers that specifically target the qNSC population (e.g., GLAST-CreERT2) along with single-cell RNA-seq will be required to definitively confirm this hypothesis.

The studies examining niche exhaustion also reveal differences between the SGZ and SVZ. Although the SGZ niche exhibits exhaustion by 8 weeks, there is no exhaustion in the SVZ at 8 weeks. We assessed the phenotype in the SVZ, particularly proliferation of aNSCs and neuroblasts, as well as cell death. Our data reveal that, in TKO, there is significant proliferation of neuroblasts in the SVZ at 4 and 8 weeks; however, there is a gradual decline at 8 versus 4 wpi. We also find an increase in cell death that persists at 8 weeks but at a lower level, resulting in a reduction in cell numbers in the SVZ. Although these results clearly underline a reduction in the size of the NSC/progenitor pool in the SVZ and suggest that niche exhaustion may indeed occur, future experiments (including birthdating studies) should examine the phenotype after longer time points and evaluate whether niche exhaustion also occurs in the SVZ.

Although loss of pocket proteins or their E2F1/3 targets results in dramatic gene expression changes identified by RNA-seq, it is also important to note that manipulation of the Rb-E2F axis results in a change in the cellular composition of the neurogenic niche. Thus, a significant proportion of the DEGs identified could be due to indirect effects rather than direct changes in Rb-E2F target gene regulation. Identification of direct Rb-E2F target genes among the DEGs and regulatory pathways will require validation and manipulation in future studies.

We describe an important function of Rb family proteins and their target activator E2Fs1/3 in regulation of NSC activation and quiescence. We demonstrate how transcriptional signatures of quiescence and activation among adult NSCs are coordinated with cell cycle control and show that the Rb/E2F axis serves as a key regulator of the molecular program instructing adult NSC exit from and re-entry into quiescence, essential for niche maintenance and, ultimately, adult neurogenesis.

STAR★METHODS

Detailed methods are provided in the online version of this paper and include the following:

- KEY RESOURCES TABLE
- RESOURCE AVAILABILITY
  - Lead contact
  - Materials availability
  - Data and code availability
- EXPERIMENTAL MODEL AND SUBJECT DETAILS
  - Animals
  - Primary cell cultures
  - Cell lines
- METHOD DETAILS
  - Perfusion, freezing, and sectioning
  - Immunohistochemistry and imaging
  - FACS and RNA isolation
  - qRT-PCR
  - RNASeq
  - Bioinformatic analysis
  - Network analysis
  - Lentiviral vectors
  - Stereotaxic injections
  - Western Blot
  - ChIP
  - ChIP-seq analysis
- QUANTIFICATION AND STATISTICAL ANALYSIS

SUPPLEMENTAL INFORMATION

Supplemental information can be found online at https://doi.org/10.1016/j.celrep.2022.111578.

ACKNOWLEDGMENTS

This work was supported by core facilities at the University of Ottawa, including Surgical Core; Dr. Vera Tang, Flow Cytometry and Virometry Core; Cell Biology and Image Acquisition Core; facilities at the Ottawa Hospital Research Institute, including the Flow Cytometry and Cell Sorting Facility and StemCore Laboratories; and The Centre for Applied Genomics at The Hospital for Sick Children, Toronto. This work was funded by CIHR grants (to R.S.S.); Belgian National Funds for Scientific Research (FRS-FNRS, Belgium), the Fondation Léon Fredericq (ULiège, Belgium), the Fonds spéciaux (ULiège, Belgium) (to R.V.); the University Research Board, American University of Beirut (URB), the Mamdouha El-Sayed Bobst Deanship Fund (FAS) at American University of Beirut (AUB), and the Lebanese National Council for Scientific Research (CNRS-L) (to N.G.); and an Ontario Graduate Scholarship (to B.C.F.).

AUTHOR CONTRIBUTIONS

Conceptualization and methods, B.C.F., I.C., S.P., A. Clark, N.G., R.V., and R.S.S.; investigation, B.C.F., I.C., M.A.I., S.P., J.B., D.O., E.Y., A.T.B., N.A.,

A. Carter, A. Clark, N.G., and R.V.; resources, G.L., D.S.P., and R.S.S.; writing, B.C.F., I.C., and R.S.S.; review, all authors.

DECLARATION OF INTERESTS

The authors declare no competing interests.

Received: January 7, 2022
Revised: August 11, 2022
Accepted: October 7, 2022
Published: November 1, 2022

REFERENCES

Ajioka, I., Martins, R.A.P., Bayazitov, I.T., Donovan, S., Johnson, D.A., Frase, S., Cicero, S.A., Boyd, K., Zakharenko, S.S., and Dyer, M.A. (2007). Differentiated horizontal interneurons clonally expand to form metastatic retinoblastoma in mice. Cell *131*, 378–390. https://doi.org/10.1016/j.cell.2007.09.036.

Andersen, J., Urban, N., Achimastou, A., Ito, A., Simic, M., Ullom, K., Martynoga, B., Lebel, M., Göritz, C., Frisén, J., et al. (2014). A transcriptional mechanism integrating inputs from extracellular signals to activate hippocampal stem cells. Neuron *83*, 1085–1097. https://doi.org/10.1016/j.neuron.2014.08.004.

Andrews, S., Krueger, F., Segonds-Pichon, A., Biggins, L., Krueger, C., and Wingett, S. (2012). FastQC.

Ballas, N., Grunseich, C., Lu, D.D., Speh, J.C., and Mandel, G. (2005). REST and its corepressors mediate plasticity of neuronal gene chromatin throughout neurogenesis. Cell *121*, 645–657. https://doi.org/10.1016/j.cell.2005.03.013.

Basak, O., Krieger, T.G., Muraro, M.J., Wiebrands, K., Stange, D.E., Frias-Aldeguer, J., Rivron, N.C., van de Wetering, M., van Es, J.H., van Oudenaarden, A., et al. (2018). Troy+ brain stem cells cycle through quiescence and regulate their number by sensing niche occupancy. Proc. Natl. Acad. Sci. USA *115*, E610–E619. https://doi.org/10.1073/pnas.1715911114.

Bergsland, M., Werme, M., Malewicz, M., Perlmann, T., and Muhr, J. (2006). The establishment of neuronal properties is controlled by Sox4 and Sox11. Genes Dev. *20*, 3475–3486. https://doi.org/10.1101/gad.403406.

Burkhart, D.L., Ngai, L.K., Roake, C.M., Viatour, P., Thangavel, C., Ho, V.M., Knudsen, E.S., and Sage, J. (2010). Regulation of RB transcription in vivo by RB family members. Mol. Cell Biol. *30*, 1729–1745. https://doi.org/10.1128/mcb.00952-09.

Callaghan, D.A., Dong, L., Callaghan, S.M., Hou, Y.X., Dagnino, L., and Slack, R.S. (1999). Neural precursor cells differentiating in the absence of Rb exhibit delayed terminal mitosis and deregulated E2F 1 and 3 activity. Dev. Biol. *207*, 257–270. https://doi.org/10.1006/dbio.1998.9162.

Chen, D., Pacal, M., Wenzel, P., Knoepfler, P.S., Leone, G., and Bremner, R. (2009). Division and apoptosis of E2f-deficient retinal progenitors. Nature *462*, 925–929. https://doi.org/10.1038/nature08544.

Chen, Z.-F., Paquette, A.J., and Anderson, D.J. (1998). NRSF/REST is required in vivo for repression of multiple neuronal target genes during embryogenesis. Nat. Genet. *20*, 136–142. https://doi.org/10.1038/2431.

Chong, J.A., Tapia-Ramírez, J., Kim, S., Toledo-Aral, J.J., Zheng, Y., Boutros, M.C., Altshuller, Y.M., Frohman, M.A., Kraner, S.D., and Mandel, G. (1995). REST: a mammalian silencer protein that restricts sodium channel gene expression to neurons. Cell *80*, 949–957. https://doi.org/10.1016/0092-8674(95)90298-8.

Chong, J.-L., Wenzel, P.L., Sáenz-Robles, M.T., Nair, V., Ferrey, A., Hagan, J.P., Gomez, Y.M., Sharma, N., Chen, H.-Z., Ouseph, M., et al. (2009). E2f1-3 switch from activators in progenitor cells to repressors in differentiating cells. Nature *462*, 930–934. https://doi.org/10.1038/nature08677.

Cicero, S.A., Johnson, D., Reyntjens, S., Frase, S., Connell, S., Chow, L.M.L., Baker, S.J., Sorrentino, B.P., and Dyer, M.A. (2009). Cells previously identified as retinal stem cells are pigmented ciliary epithelial cells. Proc. Natl. Acad. Sci. USA *106*, 6685–6690. https://doi.org/10.1073/pnas.0901596106.

Codega, P., Silva-Vargas, V., Paul, A., Maldonado-Soto, A.R., Deleo, A.M., Pastrana, E., and Doetsch, F. (2014). Prospective identification and purification of quiescent adult neural stem cells from their in vivo niche. Neuron *82*, 545–559. https://doi.org/10.1016/j.neuron.2014.02.039.

Cooper-Kuhn, C.M., Vroemen, M., Brown, J., Ye, H., Thompson, M.A., Winkler, J., and Kuhn, H.G. (2002). Impaired adult neurogenesis in mice lacking the transcription factor E2F1. Mol. Cell. Neurosci. *21*, 312–323. https://doi.org/10.1006/mcne.2002.1176.

Davis, C.A., Hitz, B.C., Sloan, C.A., Chan, E.T., Davidson, J.M., Gabdank, I., Hilton, J.A., Jain, K., Baymuradov, U.K., Narayanan, A.K., et al. (2018). The Encyclopedia of DNA elements (ENCODE): data portal update. Nucleic Acids Res. *46*, D794–D801. https://doi.org/10.1093/nar/gkx1081.

Delgado, A.C., Maldonado-Soto, A.R., Silva-Vargas, V., Mizrak, D., von Känel, T., Tan, K.R., Paul, A., Madar, A., Cuervo, H., Kitajewski, J., et al. (2021). Release of stem cells from quiescence reveals gliogenic domains in the adult mouse brain. Science *372*, 1205–1209. https://doi.org/10.1126/science.abg8467.

Dunham, I., Kundaje, A., Aldred, S.F., Collins, P.J., Davis, C.A., Doyle, F., Epstein, C.B., Frietze, S., Harrow, J., Kaul, R., et al. (2012). An integrated encyclopedia of DNA elements in the human genome. Nature *489*, 57–74. https://doi.org/10.1038/nature11247.

Durinck, S., Spellman, P.T., Birney, E., and Huber, W. (2009). Mapping identifiers for the integration of genomic datasets with the R/Bioconductor package biomaRt. Nat. Protoc. *4*, 1184–1191. https://doi.org/10.1038/nprot.2009.97.

Encinas, J.M., Michurina, T.V., Peunova, N., Park, J.-H., Tordo, J., Peterson, D.A., Fishell, G., Koulakov, A., and Enikolopov, G. (2011). Division-coupled astrocytic differentiation and age-related depletion of neural stem cells in the adult Hippocampus. Cell Stem Cell *8*, 566–579. https://doi.org/10.1016/j.stem.2011.03.010.

Ferland, R.J., Batiz, L.F., Neal, J., Lian, G., Bundock, E., Lu, J., Hsiao, Y.-C., Diamond, R., Mei, D., Banham, A.H., et al. (2009). Disruption of neural progenitors along the ventricular and subventricular zones in periventricular heterotopia. Hum. Mol. Genet. *18*, 497–516. https://doi.org/10.1093/hmg/ddn377.

Field, S.J., Tsai, F.-Y., Kuo, F., Zubiaga, A.M., Kaelin, W.G., Livingston, D.M., Orkin, S.H., and Greenberg, M.E. (1996). E2F-1 functions in mice to promote apoptosis and suppress proliferation. Cell *85*, 549–561. https://doi.org/10.1016/s0092-8674(00)81255-6.

Friend, S.H., Bernards, R., Rogelj, S., Weinberg, R.A., Rapaport, J.M., Albert, D.M., and Dryja, T.P. (1986). A human DNA segment with properties of the gene that predisposes to retinoblastoma and osteosarcoma. Nature *323*, 643–646. https://doi.org/10.1038/323643a0.

Gao, Z., Ure, K., Ding, P., Nashaat, M., Yuan, L., Ma, J., Hammer, R.E., and Hsieh, J. (2011). The master negative regulator REST/NRSF controls adult neurogenesis by restraining the neurogenic program in quiescent stem cells. J. Neurosci. *31*, 9772–9786. https://doi.org/10.1523/jneurosci.1604-11.2011.

Gonçalves, J.T., Schafer, S.T., and Gage, F.H. (2016). Adult neurogenesis in the Hippocampus: from stem cells to behavior. Cell *167*, 897–914. https://doi.org/10.1016/j.cell.2016.10.021.

Hodge, R.D., Nelson, B.R., Kahoud, R.J., Yang, R., Mussar, K.E., Reiner, S.L., and Hevner, R.F. (2012). Tbr2 is essential for hippocampal lineage progression from neural stem cells to intermediate progenitors and neurons. J. Neurosci. *32*, 6275–6287. https://doi.org/10.1523/jneurosci.0532-12.2012.

Ignatiadis, N., Klaus, B., Zaugg, J.B., and Huber, W. (2016). Data-driven hypothesis weighting increases detection power in genome-scale multiple testing. Nat. Methods *13*, 577–580. https://doi.org/10.1038/nmeth.3885.

Iqbal, M.A., Fong, B.C., and Slack, R.S. (2022). Direct FACS isolation of neural stem/progenitor lineages from the adult brain. Methods Mol. Biol. *2515*, 117–127. https://doi.org/10.1007/978-1-0716-2409-8_8.

Jaafar, C., Omais, S., Al Lafi, S., El Jamal, N., Noubani, M., Skaf, L., and Ghanem, N. (2016). Role of Rb during neurogenesis and axonal guidance in the developing olfactory system. Front. Mol. Neurosci. *9*, 81, 15. https://doi.org/10.3389/fnmol.2016.00081.

Janky, R., Verfaillie, A., Imrichová, H., Van de Sande, B., Standaert, L., Christiaens, V., Hulselmans, G., Herten, K., Naval Sanchez, M., Potier, D., et al. (2014). iRegulon: from a gene list to a gene regulatory network using large motif and track collections. PLoS Comput. Biol. *10*, 10037311–e1003819. https://doi.org/10.1371/journal.pcbi.1003731.

Jiang, Z., Deng, T., Jones, R., Li, H., Herschkowitz, J.I., Liu, J.C., Weigman, V.J., Tsao, M.-S., Lane, T.F., Perou, C.M., and Zacksenhaus, E. (2010). Rb deletion in mouse mammary progenitors induces luminal-B or basal-like/EMT tumor subtypes depending on p53 status. J. Clin. Invest. *120*, 3296–3309. https://doi.org/10.1172/jci41490.

Jørgensen, H.F., Terry, A., Beretta, C., Pereira, C.F., Leleu, M., Chen, Z.-F., Kelly, C., Merkenschlager, M., and Fisher, A.G. (2009). REST selectively represses a subset of RE1-containing neuronal genes in mouse embryonic stem cells. Development *136*, 715–721. https://doi.org/10.1242/dev.028548.

Julian, L.M., Liu, Y., Pakenham, C.A., Dugal-Tessier, D., Ruzhynsky, V., Bae, S., Tsai, S.-Y., Leone, G., Slack, R.S., and Blais, A. (2016). Tissue-specific targeting of cell fate regulatory genes by E2f factors. Cell Death Differ. *23*, 565–575. https://doi.org/10.1038/cdd.2015.36.

Julian, L.M., Vandenbosch, R., Pakenham, C.A., Andrusiak, M.G., Nguyen, A.P., McClellan, K.A., Svoboda, D.S., Lagace, D.C., Park, D.S., Leone, G., et al. (2013). Opposing regulation of Sox2 by cell-cycle effectors E2f3a and E2f3b in neural stem cells. Cell Stem Cell *12*, 440–452. https://doi.org/10.1016/j.stem.2013.02.001.

Kareta, M.S., Gorges, L.L., Hafeez, S., Benayoun, B.A., Marro, S., Zmoos, A.-F., Cecchini, M.J., Spacek, D., Batista, L.F.Z., O'Brien, M., et al. (2015). Inhibition of pluripotency networks by the Rb tumor suppressor restricts reprogramming and tumorigenesis. Cell Stem Cell *16*, 39–50. https://doi.org/10.1016/j.stem.2014.10.019.

Kim, D., Paggi, J.M., Park, C., Bennett, C., and Salzberg, S.L. (2019). Graph-based genome alignment and genotyping with HISAT2 and HISAT-genotype. Nat. Biotechnol. *37*, 907–915. https://doi.org/10.1038/s41587-019-0201-4.

Kim, E., Cheng, Y., Bolton-Gillespie, E., Cai, X., Ma, C., Tarangelo, A., Le, L., Jambhekar, M., Raman, P., Hayer, K.E., et al. (2017). Rb family proteins enforce the homeostasis of quiescent hematopoietic stem cells by repressing Socs3 expression. J. Exp. Med. *214*, 1901–1912. https://doi.org/10.1084/jem.20160719.

Kwon, J.S., Everetts, N.J., Wang, X., Wang, W., Della Croce, K., Xing, J., and Yao, G. (2017). Controlling depth of cellular quiescence by an Rb-E2F network switch. Cell Rep. *20*, 3223–3235. https://doi.org/10.1016/j.celrep.2017.09.007.

Lee, W.-H., Shew, J.-Y., Hong, F.D., Sery, T.W., Donoso, L.A., Young, L.-J., Bookstein, R., and Lee, E.Y. (1987). The retinoblastoma susceptibility gene encodes a nuclear phosphoprotein associated with DNA binding activity. Nature *329*, 642–645. https://doi.org/10.1038/329642a0.

Lepagnol-Bestel, A.-M., Zvara, A., Maussion, G., Quignon, F., Ngimbous, B., Ramoz, N., Imbeaud, S., Loe-Mie, Y., Benihoud, K., Agier, N., et al. (2009). DYRK1A interacts with the REST/NRSF-SWI/SNF chromatin remodelling complex to deregulate gene clusters involved in the neuronal phenotypic traits of Down syndrome. Hum. Mol. Genet. *18*, 1405–1414. https://doi.org/10.1093/hmg/ddp047.

Liao, Y., Smyth, G.K., and Shi, W. (2014). featureCounts: an efficient general purpose program for assigning sequence reads to genomic features. Bioinformatics *30*, 923–930. https://doi.org/10.1093/bioinformatics/btt656.

Litovchick, L., Sadasivam, S., Florens, L., Zhu, X., Swanson, S.K., Velmurugan, S., Chen, R., Washburn, M.P., Liu, X.S., and DeCaprio, J.A. (2007). Evolutionarily conserved multisubunit RBL2/p130 and E2F4 protein complex represses human cell cycle-dependent genes in quiescence. Mol. Cell *26*, 539–551. https://doi.org/10.1016/j.molcel.2007.04.015.

Liu, Y., Chu, A., Chakroun, I., Islam, U., and Blais, A. (2010). Cooperation between myogenic regulatory factors and SIX family transcription factors is important for myoblast differentiation. Nucleic Acids Res. *38*, 6857–6871. https://doi.org/10.1093/nar/gkq585.

Love, M.I., Huber, W., and Anders, S. (2014). Moderated estimation of fold change and dispersion for RNA-seq data with DESeq2. Genome Biol. *15*, 550–648. https://doi.org/10.1186/s13059-014-0550-8.

McClellan, K.A., Ruzhynsky, V.A., Douda, D.N., Vanderluit, J.L., Ferguson, K.L., Chen, D., Bremner, R., Park, D.S., Leone, G., and Slack, R.S. (2007). Unique requirement for Rb/E2F3 in neuronal migration: evidence for cell cycle-independent functions. Mol. Cell Biol. *27*, 4825–4843. https://doi.org/10.1128/mcb.02100-06.

McGann, J.C., Spinner, M., Garg, S.K., Mullendorf, K., Woltjer, R.L., and Mandel, G. (2020). Genome-wide assessment of REST binding profiles reveals distinctions between human and mouse hippocampus. Preprint at bioRxiv. https://doi.org/10.1101/2020.07.07.192229.

Merico, D., Isserlin, R., Stueker, O., Emili, A., and Bader, G.D. (2010). Enrichment Map: a network-based method for gene-set enrichment visualization and interpretation. PLoS One *5*, e13984. https://doi.org/10.1371/journal.pone.0013984.

Miles, D.K., and Kernie, S.G. (2008). Hypoxic-ischemic brain injury activates early hippocampal stem/progenitor cells to replace vulnerable neuroblasts. Hippocampus *18*, 793–806. https://doi.org/10.1002/hipo.20439.

Morris, E.J., and Dyson, N.J. (2001). Retinoblastoma protein partners. Adv. Cancer Res. *82*, 1–54. https://doi.org/10.1016/s0065-230x(01)82001-7.

Mu, L., Berti, L., Masserdotti, G., Covic, M., Michaelidis, T.M., Doberauer, K., Merz, K., Rehfeld, F., Haslinger, A., Wegner, M., et al. (2012). SoxC transcription factors are required for neuronal differentiation in adult hippocampal neurogenesis. J. Neurosci. *32*, 3067–3080. https://doi.org/10.1523/jneurosci.4679-11.2012.

Mukherjee, S., Brulet, R., Zhang, L., and Hsieh, J. (2016). REST regulation of gene networks in adult neural stem cells. Nat. Commun. *7*, 13360–13414. https://doi.org/10.1038/ncomms13360.

Naser, R., Vandenbosch, R., Omais, S., Hayek, D., Jaafar, C., Al Lafi, S., Saliba, A., Baghdadi, M., Skaf, L., and Ghanem, N. (2016). Role of the Retinoblastoma protein, Rb, during adult neurogenesis in the olfactory bulb. Sci. Rep. *6*, 20230. https://doi.org/10.1038/srep20230.

Obernier, K., and Alvarez-Buylla, A. (2019). Neural stem cells: origin, heterogeneity and regulation in the adult mammalian brain. Development *146*, dev156059. https://doi.org/10.1242/dev.156059.

Raudvere, U., Kolberg, L., Kuzmin, I., Arak, T., Adler, P., Peterson, H., and Vilo, J. (2019). g:Profiler: a web server for functional enrichment analysis and conversions of gene lists (2019 update). Nucleic Acids Res. *47*, W191–W198. https://doi.org/10.1093/nar/gkz369.

Reimand, J., Isserlin, R., Voisin, V., Kucera, M., Tannus-Lopes, C., Rostamianfar, A., Wadi, L., Meyer, M., Wong, J., Xu, C., et al. (2019). Pathway enrichment analysis and visualization of omics data using g:Profiler, GSEA, Cytoscape and EnrichmentMap. Nat. Protoc. *14*, 482–517. https://doi.org/10.1038/s41596-018-0103-9.

Reimand, J., Kull, M., Peterson, H., Hansen, J., and Vilo, J. (2007). g:Profiler—a web-based toolset for functional profiling of gene lists from large-scale experiments. Nucleic Acids Res. *35*, W193–W200. https://doi.org/10.1093/nar/gkm226.

Reynolds, B.A., and Weiss, S. (1992). Generation of neurons and astrocytes from isolated cells of the adult mammalian central nervous system. Science (New York, N.Y.) *255*, 1707–1710. https://doi.org/10.1126/science.1553558.

Robinson, J.T., Thorvaldsdóttir, H., Winckler, W., Guttman, M., Lander, E.S., Getz, G., and Mesirov, J.P. (2011). Integrative genomics viewer. Nat. Biotechnol. *29*, 24–26. https://doi.org/10.1038/nbt.1754.

Sage, J., Mulligan, G.J., Attardi, L.D., Miller, A., Chen, S., Williams, B., Theodorou, E., and Jacks, T. (2000). Targeted disruption of the three Rb-related genes leads to loss of G1 control and immortalization. Genes Dev. *14*, 3037–3050. https://doi.org/10.1101/gad.843200.

Sage, J., Miller, A.L., Pérez-Mancera, P.A., Wysocki, J.M., and Jacks, T. (2003). Acute mutation of retinoblastoma gene function is sufficient for cell cycle re-entry. Nature *424*, 223–228. https://doi.org/10.1038/nature01764.

Schindelin, J., Arganda-Carreras, I., Frise, E., Kaynig, V., Longair, M., Pietzsch, T., Preibisch, S., Rueden, C., Saalfeld, S., Schmid, B., et al. (2012). Fiji: an open-source platform for biological-image analysis. Nat. Methods *9*, 676–682. https://doi.org/10.1038/nmeth.2019.

Schneider, C.A., Rasband, W.S., and Eliceiri, K.W. (2012). NIH Image to ImageJ: 25 years of image analysis. Nat. Methods *9*, 671–675. https://doi.org/10.1038/nmeth.2089.

Schoenherr, C.J., and Anderson, D.J. (1995). The neuron-restrictive silencer factor (NRSF): a coordinate repressor of multiple neuron-specific genes. Science *267*, 1360–1363. https://doi.org/10.1126/science.7871435.

Shannon, P., Markiel, A., Ozier, O., Baliga, N.S., Wang, J.T., Ramage, D., Amin, N., Schwikowski, B., and Ideker, T. (2003). Cytoscape: a software environment for integrated models of biomolecular interaction networks. Genome Res. *13*, 2498–2504. https://doi.org/10.1101/gr.1239303.

Soldati, C., Caramanica, P., Burney, M.J., Toselli, C., Bithell, A., Augusti-Tocco, G., Stanton, L.W., Biagioni, S., Buckley, N.J., and Cacci, E. (2015). RE1 silencing transcription factor/neuron-restrictive silencing factor regulates expansion of adult mouse subventricular zone-derived neural stem/progenitor cells in vitro. J. Neurosci. Res. *93*, 1203–1214. https://doi.org/10.1002/jnr.23572.

Srinivas, S., Watanabe, T., Lin, C.-S., William, C.M., Tanabe, Y., Jessell, T.M., and Costantini, F. (2001). Cre reporter strains produced by targeted insertion of EYFP and ECFP into the ROSA26 locus. BMC Dev. Biol. *1*, 4. https://doi.org/10.1186/1471-213x-1-4.

TANG, Y., GARSON, K., LI, L., and VANDERHYDEN, B.C. (2015). Optimization of lentiviral vector production using polyethylenimine-mediated transfection. Oncol. Lett. *9*, 55–62. https://doi.org/10.3892/ol.2014.2684.

Team R.C (2021). R: A Language and Environment for Statistical Computing.

Urbán, N., van den Berg, D.L.C., Forget, A., Andersen, J., Demmers, J.A.A., Hunt, C., Ayrault, O., and Guillemot, F. (2016). Return to quiescence of mouse neural stem cells by degradation of a proactivation protein. Science *353*, 292–295. https://doi.org/10.1126/science.aaf4802.

Urbán, N., Blomfield, I.M., and Guillemot, F. (2019). Quiescence of adult mammalian neural stem cells: a highly regulated rest. Neuron *104*, 834–848. https://doi.org/10.1016/j.neuron.2019.09.026.

Vandenbosch, R., Clark, A., Fong, B.C., Omais, S., Jaafar, C., Dugal-Tessier, D., Dhaliwal, J., Lagace, D.C., Park, D.S., Ghanem, N., and Slack, R.S. (2016). RB regulates the production and the survival of newborn neurons in the embryonic and adult dentate gyrus. Hippocampus *26*, 1379–1392. https://doi.org/10.1002/hipo.22613.

Vanderluit, J.L., Ferguson, K.L., Nikoletopoulou, V., Parker, M., Ruzhynsky, V., Alexson, T., McNamara, S.M., Park, D.S., Rudnicki, M., and Slack, R.S. (2004). p107 regulates neural precursor cells in the mammalian brain. J. Cell Biol. *166*, 853–863. https://doi.org/10.1083/jcb.200403156.

Vanderluit, J.L., Wylie, C.A., McClellan, K.A., Ghanem, N., Fortin, A., Callaghan, S., MacLaurin, J.G., Park, D.S., and Slack, R.S. (2007). The Retinoblastoma family member p107 regulates the rate of progenitor commitment to a neuronal fate. J. Cell Biol. *178*, 129–139. https://doi.org/10.1083/jcb.200703176.

Viatour, P., Ehmer, U., Saddic, L.A., Dorrell, C., Andersen, J.B., Lin, C., Zmoos, A.-F., Mazur, P.K., Schaffer, B.E., Ostermeier, A., et al. (2011). Notch signaling inhibits hepatocellular carcinoma following inactivation of the RB pathway. J. Exp. Med. *208*, 1963–1976. https://doi.org/10.1084/jem.20110198.

Viatour, P., Somervaille, T.C., Venkatasubrahmanyam, S., Kogan, S., McLaughlin, M.E., Weissman, I.L., Butte, A.J., Passegué, E., and Sage, J. (2008). Hematopoietic stem cell quiescence is maintained by compound contributions of the retinoblastoma gene family. Cell Stem Cell *3*, 416–428. https://doi.org/10.1016/j.stem.2008.07.009.

Wang, X., Seekaew, P., Gao, X., and Chen, J. (2016). Traumatic brain injury stimulates neural stem cell proliferation via mammalian target of rapamycin signaling pathway activation. ENeuro *3*, ENEURO.0162-16.2016. https://doi.org/10.1523/eneuro.0162-16.2016.

Wu, L., Timmers, C., Maiti, B., Saavedra, H.I., Sang, L., Chong, G.T., Nuckolls, F., Giangrande, P., Wright, F.A., Field, S.J., et al. (2001). The E2F1–3 transcription factors are essential for cellular proliferation. Nature *414*, 457–462. https://doi.org/10.1038/35106593.

Xi, Y., Dhaliwal, J.S., Ceizar, M., Vaculik, M., Kumar, K.L., and Lagace, D.C. (2016). Knockout of Atg5 delays the maturation and reduces the survival of adult-generated neurons in the hippocampus. Cell Death Dis. *7*, e2127. https://doi.org/10.1038/cddis.2015.406.

Zhou, G., Soufan, O., Ewald, J., Hancock, R.E.W., Basu, N., and Xia, J. (2019). NetworkAnalyst 3.0: a visual analytics platform for comprehensive gene expression profiling and meta-analysis. Nucleic Acids Res. *47*, W234–W241. https://doi.org/10.1093/nar/gkz240.

STAR★METHODS

KEY RESOURCES TABLE

REAGENT or RESOURCE	SOURCE	IDENTIFIER
Antibodies		
E2F1 (Rabbit; ChIP)	Santa Cruz	CAT#sc-193; RRID:AB_631394
E2F3 (Rabbit; ChIP)	Abcam	CAT#ab-50917; RRID:AB_869541
E2F4 (Rabbit; ChIP)	Santa Cruz	CAT#sc-1082; RRID:AB_2097104
E2F4 (Rabbit; ChIP)	NovusBio	CAT#NBP1-21374; RRID:AB_1660082
IgG (Rabbit; ChIP)	Sigma-Aldrich	CAT#I8140; RRID:AB_1163661
p130 (Rabbit; ChIP)	Santa Cruz	CAT#sc-317; RRID:AB_632093
REST (Rabbit; ChIP)	Millipore	CAT#07–579; RRID:AB_310728
p107 (Rabbit; WB, ChIP)	Santa Cruz	CAT#sc-318; RRID:AB_2175428
p130 (Mouse; WB, ChIP)	BD Biosciences	CAT#610262; RRID:AB_397657
Rb (Rabbit; WB, ChIP)	Santa Cruz	CAT#sc-50; RRID:AB_632339
Rb (Rabbit; WB)	Abcam	CAT#ab181616; RRID:AB_2848193
β-actin-HRP (Mouse; WB)	Santa Cruz	CAT#sc-47778; RRID:AB_626632
βIII tubulin (Rabbit; WB)	Covance	CAT#PRB 435P; RRID:AB_291637
Dcx (Rabbit; WB)	Cell Signaling	CAT#4604; RRID:AB_561007
Mash1 (Mouse; WB)	BD Biosciences	CAT#556604; RRID:AB_396479
Rest (Rabbit; WB)	Abcam	CAT#ab-21635; RRID:AB_777678
PCNA (Mouse; WB)	Santa Cruz	Cat#sc-56; RRID:AB_628110
V5-tag (Rabbit; WB)	Bethyl	CAT#A190-120A; RRID:AB_67586
β tubulin (Mouse; WB)	DSHB	CAT#E7; RRID:AB_528499
GFP (Chicken; IHC)	Abcam	CAT#ab13970; RRID:AB_300798
GFP (Rabbit; IHC)	EnCor	CAT#RPCA-GFP; RRID:AB_2572327
Nestin (Goat; IHC)	R&D Systems	CAT#AF2736; RRID:AB_416673
Nestin (Chicken; IHC)	Abcam	CAT#ab134017; RRID:AB_2753197
GFAP (Mouse; IHC)	Millipore	CAT#MAB3402; RRID:AB_94844
GFAP (Goat; IHC)	Santa Cruz	CAT#sc-6170; RRID:AB_641021
Sox2 (Goat; IHC)	Santa Cruz	CAT#sc-17320; RRID:AB_2286684
Sox2 (Goat; IHC)	Neuromics	CAT#GT15098; RRID:AB_2195800
ASCL1 (Rabbit; IHC)	Abcam	CAT#ab211327; RRID:AB_2924270
Ki67 (Rabbit; IHC)	Cell Marque	CAT#275R-16; RRID:AB_1158037
Tbr2 (Rat; IHC)	Invitrogen	CAT#14-4875-82; RRID:AB_11042577
Dcx (Goat; IHC)	Santa Cruz	CAT#SC-8066; RRID:AB_2088494
Dcx (Guinea Pig; IHC)	Millipore	CAT#AB2253; RRID:AB_1586992
Dcx (Rabbit; IHC)	Cell Signaling	CAT#4604S; RRID:AB_561007
Prox1 (Rabbit; IHC)	Millipore	CAT#AB5475; RRID:AB_177485
NeuN (Rabbit; IHC)	Millipore	CAT#MAB377; RRID:AB_2298772
mCherry (Rat; IHC)	ThermoFisher	CAT#M11217; RRID:AB_2536611
Active Caspase 3 (Rabbit; IHC)	Cell Signaling	CAT#9664S; RRID:AB_2070042
S100-β (Rabbit; IHC)	Dako	CAT#Z0311; RRID:AB_10013383
Chemicals, Peptides, and Recombinant Proteins		
Tamoxifen	Millipore Sigma	CAT#T5648
EdU	BaseClick	CAT#BCK647-IV-IM-M
Paraformaldehyde	E COM	CAT#Px0055-3
Tissue-Tek OCT Compound	VWR	CAT#25608–930

(*Continued on next page*)

Continued

REAGENT or RESOURCE	SOURCE	IDENTIFIER
DAPI	Millipore Sigma	CAT#D9542
Epredia™ Immu-Mount™	Fisher	CAT#9990412
Percoll	Millipore Sigma	CAT#GE17-0891-02
DMEM/F12	Gibco	CAT#11330–032
B27 without Vitamin A	Gibco	CAT#12587010
EGF	Millipore Sigma	CAT#E−1257
bFGF	Millipore Sigma	CAT#F-0291
heparin	Millipore Sigma	CAT#H-3149
Penicillin/Streptomycin	Gibco	CAT#1570–063
Matrigel	VWR	CAT#CACB356230
B27 with Vitamin A	Gibco	CAT#17504044
N2	Gibco	CAT#17502048
HI-FBS	Wisent	CAT#080–150
Clarity Enhanced chemiluminescence Western Blotting Substrate	Bio-Rad	CAT#1705061
Papain	Cedarlane	CAT#LS003126
DNase I	Roche	CAT#11284932001
RNaseZAP	ThermoFisher	CAT#AM9780
Critical Commercial Assays		
Arcturus® PicoPure® RNA Isolation Kit	ThermoFisher	CAT#KIT0204
Rotor-Gene SYBR® Green PCR Kit	Qiagen	CAT#204074
SMART-Seq® v4 Ultra® Low Input RNA Kit for Sequencing	Takara	CAT#634890
Nextera XT DNA Library Preparation Kit	Illumina	CAT#FC-131-1024
Deposited Data		
Gene signatures of cell clusters in the adult mouse V-SVZ	Basak et al. (2018)	GEO: GSE65970
Gene signatures of Quiescent and Activated NSC populations in the adult mouse V-SVZ	Codega et al. (2014)	GEO: GSE54653
ChIP-seq data on REST in rat cells (QNP and TAP)	Mukherjee et al. (2016)	SRA: SRP060618
ChIP-seq data on Rest in human cells	ENCODE	SRA: SRP008797
ChIP-seq data on Rest in human cells	ENCODE	SRA: SRP012412
RNA-seq data on Rb-THC, Rb-TKO, E2F1/3-HET and E2F1/3-DKO in mouse neural stem cells	This paper	GEO: GSE190766
Experimental Models: Cell Lines		
Micro-dissected and FACS-isolated SVZ YFP + NSCs	N/A	N/A
Micro-dissected SVZ NSCs	N/A	N/A
293T HEK Cells	ATCC	CRL3216
Experimental Models: Organisms/Strains		
Mouse: Rb-TKO (Rb conditional mutant; p107 −/−; p130 conditional mutant) on129Sv/J X C57/BL6 background	Dr. Julien Sage	Viatour et al. (2008)
Mouse:E2F1/3-DKO(E2F1 −/−; E2F3 conditional mutant)onFVB/N X 129Sv/J X C57/BL6 background	Dr. Gustavo Leone	E2F1: Field et al. (1996); E2F3: Wu et al. (2001)

(*Continued on next page*)

Continued

REAGENT or RESOURCE	SOURCE	IDENTIFIER
Mouse: Nestin-CreER^{T2}; R26-stop-enhanced yellow fluorescent protein (YFP)	Dr. Suzanne Baker	Cicero et al. (2009)
Oligonucleotides		
Genotyping Primers, see Table S2	N/A	N/A
qRT-PCR Primers, see Table S3	N/A	N/A
ChIP Primers, see Table S4	N/A	N/A
Recombinant DNA		
pLVX-EF1a-IRES-mCherry	Clontech	631987
Software and Algorithms		
Fiji	Schindelin et al. (2012)	https://fiji.sc
FastQC	Andrews et al. (2012)	https://www.bioinformatics.babraham.ac.uk/projects/fastqc/
HiSat2	Kim et al. (2019)	http://daehwankimlab.github.io/hisat2/
IGV	Robinson et al. (2011)	https://software.broadinstitute.org/software/igv/
featureCounts	Liao et al. (2014)	http://subread.sourceforge.net
R 3.5.3	Team R.C, 2021	https://www.r-project.org
DESeq2	Love et al. (2014)	https://bioconductor.org/packages/release/bioc/html/DESeq2.html
IHW	Ignatiadis et al. (2016)	https://bioconductor.org/packages/release/bioc/html/IHW.html
biomaRt	Durinck et al. (2009)	https://bioconductor.org/packages/release/bioc/html/biomaRt.html
g:Profiler	Raudvere et al. (2019); Reimand et al. (2007)	https://biit.cs.ut.ee/gprofiler/gost
Cytoscape 3.8.2	Shannon et al. (2003)	https://cytoscape.org
Enrichment Map	Merico et al. (2010)	https://www.baderlab.org/Software/EnrichmentMap
iRegulon	Janky et al. (2014)	http://iregulon.aertslab.org
NetworkAnalyst	Zhou et al. (2019)	https://www.networkanalyst.ca
ImageJ	Schneider et al. (2012)	https://imagej.net/software/imagej/
Prism 9.4.0	GraphPad	https://www.graphpad.com/scientific-software/prism/

RESOURCE AVAILABILITY

Lead contact

Further information and requests for resources and reagents should be directed to and will be fulfilled by the lead contact, Ruth Slack (rslack@uottawa.ca)

Materials availability

This study did not generate new unique reagents.

Data and code availability

- The data discussed in this publication have been deposited in NCBI's Gene Expression Omnibus and are accessible through GEO Series accession number GEO: GSE190766.
- The published article includes all datasets generated or analyzed during this study and no new code was produced.
- Any additional information required to reanalyze the data reported in this paper is available from the lead contact upon request.

EXPERIMENTAL MODEL AND SUBJECT DETAILS

Animals

All experiments were approved by the Animal Care Ethics Committee of the University of Ottawa and adhered to the Guidelines of the Canadian Council on Animal Care.

Rb-TKO (Rb conditional mutant; p107 −/−; p130 conditional mutant) mice were provided by Dr. Julien Sage (Viatour et al., 2008), and crossed with Nestin-CreER^{T2} (Cicero et al., 2009); R26-stop-enhanced yellow fluorescent protein (YFP) (Srinivas et al., 2001) mice. All Rb-TKO mice were maintained on a mixed 129Sv/J X C57/BL6 background; Rb-THC mice were generated by crossing Rb-TKO mice with wild-type 129Sv/J X C57/BL6 mice from Charles River to generate a triple-heterozygous control.

E2F1/3-DKO (E2F1 −/− (Field et al., 1996); E2F3 conditional mutant (Wu et al., 2001)) mice were provided by Dr. Gustavo Leone, and crossed with Nestin-CreER^{T2};R26EYFP mice described above. All E2F1/3-DKO mice were maintained on a mixed FVB/N X 129Sv/J X C57/BL6 background; E2F1/3-HET mice were generated by crossing E2F1/3-DKO mice with wild-type FVB/N X 129Sv/J X C57/BL6 mice from Charles River to generate a double-heterozygous control.

Animals were genotyped according to standard protocols with previously published primers, listed in Table S2. All Nestin-CreER^{T2} animals used were heterozygotes for Cre expression. In all experiments, both females and males were used; all animals were 6–10 weeks old upon initial intervention.

For Cre induction in adult NestinCreERT2 animals, mice were administered tamoxifen (TAM) at 200 mg/kg/d for 5d (gavage; dissolved in 10% EtOH/90% corn oil), with initial weight used for dose calculation; weight after final injection was monitored, and semi-weekly wellness checks were performed until euthanization. Animals in Figures S1B and S1C were administered TAM at 150 mg/kg/d for 5d (intraperitoneal; dissolved in 10% EtOH/90% sunflower oil), following same calculation/monitoring/wellness protocol. To analyze cell proliferation, NestinCreERT2 mice were given a single injection of EdU (50mg/kg, i.p) 2 h before euthanization and perfusion.

Primary cell cultures

YFP + cells and NSCs were isolated from SVZ tissue obtained from mice 10 days post-tamoxifen injection as previously described (Iqbal et al., 2022). Briefly, brains were micro-dissected in cold ACSF, tissue was digested in a Papain suspension (Cedarlane) and resuspended in FBS (Wisent) and DNase I (Roche), before using a 22% (v/v) PBS-buffered Percoll solution (Millipore Sigma) to achieve cells suitable for suspension. Cells were then either FACS-isolated to provide a YFP + fraction for bulk RNA-Seq or cell culture or, to compensate for the absence of FACS, rinsed in DMEM:F12 (Gibco) to remove excess Percoll from the cell surface.

Cells were plated at a concentration of 10 cells/μL in stem cell media as previously described (Reynolds and Weiss, 1992). Briefly, DMEM/F12 (Gibco) is supplemented with B27 without Vitamin A (Gibco), EGF (Sigma), bFGF (Sigma), heparin (Sigma) and Penicillin/Streptomycin (Gibco) to encourage neurosphere growth. Neurospheres were passaged after 6–7 days, up to three times, plated at a concentration of 4 cells/μL. For differentiation, plates were coated with 10% Matrigel (VWR) in serum-free media. Cells were plated as neurospheres and grown in differentiation media; DMEM/F12 supplemented with B27 with Vitamin A (Gibco), N2 (Gibco), 2% HI-FBS (Wisent) and Penicillin/Streptomycin. Cells were differentiated for 0, 1 and 3 days, with a media change on Day 2.

Cell lines

HEK-293T cells (ATCC) were maintained in Biolite cell culture treated dishes (Thermo Scientific) with DMEM (Gibco) supplemented with 1% penicillin-streptomycin and 10% FBS (Gibco) in an incubator (37°C, 5% CO2). Cell line was obtained from a high-quality source (ATCC) and cross-referenced against the ICLAC Register of Misidentified Cell Lines.

METHOD DETAILS

Perfusion, freezing, and sectioning

Tissue perfusion and fixation was performed as previously described (McClellan et al., 2007). Briefly, 4% Paraformaldehyde was prepared fresh within 2 h of perfusion. Animals were perfused transcardially, employing chilled 0.9% saline in advance of PFA. Brains were immersed in PFA overnight, followed by wash in 1X PBS and storage in 20% sucrose the following morning. Once the brains had sunken in the sucrose, they were suitable for freezing. Brains were removed from sucrose, lightly patted dry on Kimwipe, and the cerebellum removed with a razor blade to establish a flat coronal edge.

Freezing occurred in isopentane pre-chilled to between −30 and −40°C, and maintained at temperature with dry ice. PFA-fixed brains were immersed in isopentane for duration following two criteria: minimum 60 s and ceasing of bubbles from brain. Frozen brains were wrapped in aluminum foil and stored at −80 until sectioning.

For sectioning, brains were mounted on a cryostat at −24°C, using VWR Tissue-Tek OCT compound. Brains were sectioned maintaining temperature between −18 and −20°C, in 30 μm sections, skipping the OB but comprising the SVZ and hippocampal formation. Free-floating sections were collected in 1X PBS with 0.1% NaCN, into 9 wells following a 1:9 serial section pattern, separating SVZ and SGZ tissue. Brains were stored long-term in 24-well plates, under film to protect against drying out, at 4°C.

Immunohistochemistry and imaging

IHC was performed as previously described (Vandenbosch et al., 2016). Briefly, free-floating sections were triple-washed 3×/5min in 1X PBS before incubation at 4°C with primary antibodies for between overnight to 48 h. After a second triple-wash, sections were incubated with dye-coupled secondary Donkey antibodies (Jackson) and DAPI (Sigma) for between 2 h to overnight. Primary antibodies listed in Table S1, as well as secondary antibodies, were diluted in 1× PBS containing 0.1% Triton, 0.1% Tween-20. Following

a final triple-wash, sections were mounted and dried at room temperature; slides were cover-slipped with Epredia™ Immu-Mount™ (Fisher) and dried at 4°C overnight.

Sections for quantifications of colocalized cells were imaged using Zeiss LSM510, and later Zeiss LSM800 confocal microscopes, employing a 40× objective. Z-stacks spanned 10 μm of post-processing section width, with 2.0 μm spacing between Z-positions. Sections quantifying single labelling were quantified on an Olympus BX-51 microscope. Images were analyzed using Fiji (Schindelin et al., 2012).

FACS and RNA isolation

FACS was performed on isolated SVZ NSCs, suspended in DMEM/F12 (without phenol red; Invitrogen) at the University of Ottawa Flow Cytometry Core as well as OHRI StemCore Laboratories, isolating the YFP + cell population using a cutoff of 488-FL-Log-Height $\geq 10^2$.

For RNA-Seq input, cell pellets containing minimum 200,000 YFP + cells were frozen, and RNA isolated using the Arcturus® PicoPure® RNA Isolation Kit (ThermoFisher). Cell pellets were divided into four: I was sent for fragment analysis at OHRI StemCore Facility; II was used for qPCR validation of knockout or differential gene expression; III was sent for sequencing; IV was reserved as a backup.

qRT-PCR

Samples for RNA quantification were prepared using the Rotor-Gene SYBR® Green PCR Kit (Qiagen) and quantified on a Qiagen Rotor-Gene Q Real-Time PCR Machine. RNA concentrations for each primer set were normalized using standard curves prepared from wild-type adult NSCs as standard. Primers used are listed in Table S3, and RNA quantifications are expressed relative to GAPDH (normalized to 1).

RNASeq

RNA input for NGS was only considered sufficient if three criteria were met: 1) concentration $\geq$7 ng/μL, for submission of minimum 35ng of RNA, 2) 260/280 $\geq$ 2 and RQN $\geq$8.0.

RNASeq was performed at TCAG at the Hospital for Sick Children, following internal QC. Samples were run in sets of 6, reflecting 3 biological replicates. cDNA conversion used the SMART-Seq® v4 Ultra® Low Input RNA Kit for Sequencing (Clontech, now Takara), while Library Preparation used the Nextera XT DNA Library Preparation Kit (Illumina). Sequencing was performed on an Illumina Hi-Seq 2500, using a multiplexed PE126bp high output flow cell.

Bioinformatic analysis

Raw reads as FastQ files were first validated as downloads using md5sum and subjected to FastQC (Andrews et al., 2012) to ensure run quality and suitability for the standard protocol of analysis without trimming or phred scores. For alignment, FastQ files were aligned to Hisat2 GRCm38 index using HiSat2 (Kim et al., 2019) to generate BAM files. Aligned reads were visualized in IGV (Robinson et al., 2011). For read assignment, BAM files were converted to feature counts using featureCounts, part of the subread package (Liao et al., 2014), as well as the Ensembl GRCm38.101 GTF file, build dated August 2020.

Differential expression analysis of feature counts was established in R 3.5.3 (Team R.C, 2021) using DESeq2 (Love et al., 2014), and employed Independent Hypothesis Weighting using the IHW package (Ignatiadis et al., 2016). For the Rb-TKO dataset, batch correction was employed to account for batch effects distinguishing samples RB_THC_1 and RB_TKO_1, stemming from sample preparation; effects are visible in Supp.Figure S3C. Ensembl Stable IDs were converted to MGI symbols using biomaRt (Durinck et al., 2009).

Network analysis

Pathway and network enrichment analysis generally followed a published protocol (Reimand et al., 2019). Enrichment analysis with Gene Ontology: Biological Process was performed using g:GOSt and g:Convert as part of the g:Profiler toolset (Raudvere et al., 2019; Reimand et al., 2007), and visualized in Cytoscape 3.8.2 (Shannon et al., 2003) using Enrichment Map (Merico et al., 2010).

Gene regulatory network analysis was performed using iRegulon (Janky et al., 2014), analyzing a putative regulatory region spanning 20kb centred around the TSS, using a motif rankings database from 10 species; significant genes ($p < 0.05$) were used as input. ENCODE TF-gene interactions were assessed using NetworkAnalyst (Zhou et al., 2019); all genes were used as input.

Lentiviral vectors

A pLVX-EF1a-IRES-mCherry lentiviral expression vector construct was commercially obtained (Clontech 631987) and used as control. A truncated, dominant-negative REST (Bergsland et al., 2006; Chen et al., 1998) was generated, and cloned to include a V5 tag. This construct was subcloned into the expression vector to generate a pLVX-EF1a-dnREST-V5-IRES-mCherry.

Lentiviruses were produced in 293T cells using PEI and ultracentrifugation, following established protocols (TANG et al., 2015), and was resuspended in PBS into small aliquots. Live titre confirmed achieving a minimum concentration of 1.2E+09 TU/mL.

For use *in vitro*, passaged cells at P2 were infected with lentiviral particles at a multiplicity of infection (MOI) of 30, before neurosphere differentiation after 5–7 days.

Stereotaxic injections

Bilateral injections of lentivirus were performed at the uOttawa Surgery Core by Dr. Anthony Carter. In order to target the SGZ, lentiviruses were bilaterally injected into the dentate gyrus following published co-ordinates (Xi et al., 2016): −1.7mm anterior/posterior, ±1.2 mediolateral, −2.4mm dorsoventral from Bregma; injection volume was 1.0 μL, at a rate of 0.2 μL/min.

Western Blot

Cell pellets of cultured adult NSCs were solubilized in a lysis buffer containing 20 mM Tris pH 6.8, 6M urea and 0.1% SDS (Liu et al., 2010). 20 ug of proteins were separated on 10% SDS-PAGE. After transfer and blocking, membranes were incubated with primary antibodies overnight at 4°C, washed 3 times with TTTBS buffer (Tris-buffered saline, TBS with 0.05% Triton X-100 and 0.05% Tween 20), incubated with HRP-tagged secondary antibody for 1 h, and washed at room temperature. Alternatively, β-actin blot was incubated for 1 h at room temperature. Finally, signal was developed using Clarity Enhanced chemiluminescence Western Blotting Substrate (BioRad). Antibodies used in Western Blot are listed in Table S1. Western blot bands were quantified using Image J.

ChIP

ChIP assays followed by quantitative real-time PCR (qPCR) were performed as previously described (Julian et al., 2016; Liu et al., 2010). Briefly, neurosphere cultures were prepared from wild-type, Rb-THC or Rb-TKO mice at 8–10 weeks of age as described above, proliferating neurospheres were triturated, cross-linked with formaldehyde, lysed, sonicated, and centrifuged at 14,000 × g to remove cellular debris. 10 μg of 30 min cross-linked chromatin and 0.8 μg of antibodies were used in ChIP assays. Antibodies are listed in Table S1, and qPCR primers are listed in Table S4.

ChIP-seq analysis

ChIP-seq data on REST in rat cells (QNP and TAP) were performed by (Mukherjee et al., 2016) and obtained from NCBI as Short Reads Archive under accession number SRP060618. ChIP-seq data on Rest in different human cells were performed by ENCODE (Davis et al., 2018; Dunham et al., 2012) and obtained from NCBI under accession numbers SRP008797 (ECC-1, GM12878, H1-hESC, H1-neurons, HCT-116, HeLa-S3, HepG2, HL-60, k562, MCF-7, PANC-1, PFSK-1, SK-N-SH) and SRP012412 (A549, GM23338, H1-hESC, HEK293 eGFP-REST, K562, K562 eGFP-REST). Sequencing read data were analyzed following ENCODE pipeline. Conditions with more than one technical or biological replicates were combined into single FastQ files. Human data were aligned to the GRCh38 (hg38) version of the human genome, while rat data were aligned to the Rnor_6.0 (rn6) version of the rat genome.

QUANTIFICATION AND STATISTICAL ANALYSIS

For cell quantification in the adult SGZ, every ninth section throughout the DG was quantified and counts were summed and multiplied by 9 to generate an estimate of the total number of cells in the DG. For cell quantification in the adult SVZ, given the larger structure, every eighteenth section throughout the SVZ was quantified and counts were summed and multiplied by 18 to generate an estimate of the total number of cells in the SVZ.

Statistical details of all experiments can be found in the figure legends. All statistical comparisons in this study were performed using an unpaired two-tailed Student's t-test, with the exception of Figure 6F, which employs a paired two-tailed Student's t-test. Differences were considered significant with a p value of <0.05 (*), **$p < 0.01$, ***$p < 0.001$, ****$p < 0.0001$. Unless otherwise stated, all data is presented as the arithmetic mean, plus or minus the standard deviation of the mean (mean ± SD). For each experiment, a minimum of 3 animals per genotype were used, with N referring to biological replicates. Prism 9.4.0 (Graphpad) was used to perform statistical analysis.